First of all, we appreciate the reviewer's comments and suggestions. In response to the reviewer's comments, we have made relevant revisions to the manuscript. Listed below are our answers and the changes made to the manuscript according to the questions and suggestions given by the reviewer. Each comment of the reviewer (in black) is listed and followed by our responses (in blue).

Review of "Aerosol as a potential factor to control the increasing torrential rain events in urban areas over the last decades" by Seoung Soo Lee et al.

The authors investigate the role of spatial gradients in aerosol concentrations on the formation o heavy precipitation from convective clouds. They use a series of high-resolution simulations with the ARW-model with either a spatially homogeneous aerosol concentration or a spatial gradient in the aerosol concentration. Heavy precipitation coincides with the boundary between the air masses with high- and low aerosol concentration, which is also marked by large convergence. In the simulations with a spatially homogeneous aerosol concentration the convergence zones remain weaker and are less organised. The authors argue that the difference in the convergence fields is a result of larger evaporative cooling in the high-aerosol airmass leading to stronger downdrafts and surface divergence.

While the role of spatial gradients for aerosol-cloud interactions has been little explored and is an interesting topic, there are several major issues with the current manuscript, most importantly the lack of an analysis of the meso-scale circulation (see general comments). Before the manuscript can be accepted for publication these issues need to be addressed by the authors and substantial changes to the manuscript are required.

1 General comments

1. Introduction: The authors claim that the temperature and humidity forcing are homogeneous across a MCS and that spatial variability in the dynamic forcing can not explain the spatial variability in MCS intensity. However, it is well known that meso-scale circulation such as sea-breeze fronts, lake-breezes, or cold-pools have a substantial impact on the evolution of convective clouds and MCS. Also a population of clouds in the same large-scale environment will produces cells of varying intensity and at various evolution stages, which leads to a complex and varied spatial distribution. This is not adequately reflected by the statements by the authors (p. 3, l. 79-86).

   As the reviewer stated here, for the same large-scale or synoptic-scale environment, there is the variability of cloud properties in a MCS and we emphasize that this study aims to understand this

by focusing on how the aerosol variability creates the variability of cloud properties for the same synoptic-scale environment which is represented by the synoptic-scale forcings.

To state that this study focuses on aerosol variability to explain the variability of cloud properties for the same synoptic-scale environment by reflecting the comment here about mesoscale circulations or forcings, text is revised as follows:

(LL91-101 on p4)

The highly inhomogeneous distribution of precipitation means that there are highly inhomogeneous variables, processes and forcings which disrupt the synoptic-forcing-induced homogeneity of MCSs in urban areas. Some of those forcings are mesoscale forcings that show mesoscale variability and, for example, are related to phenomena such as sea-breeze fronts and lake breezes. In particular, in urban areas, due to strong heat fluxes at the surface, there is the urban heat island (UHI) effect as another example of those phenomena. Examples of those variables and processes are cold pool, rear inflow, wind shear, and mesoscale vorticity. Aerosol is also one of those variables which have large spatial variability. In particular, urban aerosol particles are produced by randomly distributed sources (e.g., traffic), which enables aerosol to have large variability in urban areas.

(LL139-144 on p5)

Motivated by the hypothesis and associated argument here, among the forcings, processes and variables which have spatial variability, this study focuses on aerosol. To examine aerosol effects on clouds and precipitation, numerical simulations are performed by using a cloud-system resolving model (CSRM) that resolves cloud-scale microphysical and dynamic processes and simulates the effect of the variability and loading of aerosol on precipitation.

2. Introduction / Conclusions (p. 4, l. 117 - p. 5, l. 123 / p. 24, l. 730 - 734) : The authors hypothesise that local variability in aerosol concentrations can drive spatial variability in precipitation. This should be more clearly highlighted as hypothesis. Also, I find this hypothesis highly unlikely as (i) convective clouds (in particularly strongly organised MCS) usually are not stationary and may ingest aerosol from various regions during their lifecycle and (ii) horizontal

gradients in aerosol are reduced by turbulent mixing during the transport to cloud base. The spatial variability discussed here appear to be of much smaller scale than those investigated with the simulations with two different aerosol-concentration air masses over an area of about 100 x 100 km.

Here, we want to emphasize that we prescribe background aerosol, its size distribution, chemical composition, and spatial gradient that are all based on observation, since for this study, we do not focus on and consider aerosol physical and chemical processes, and effects of clouds and associated convection and turbulent mixing on the background aerosol. By excluding those processes and effects, we can isolate effects of prescribed or background aerosol loading and its spatial distributions on clouds and precipitation with confidence. Note that our level of understanding of effects of background aerosol itself on precipitation in urban areas has been very low, and through the isolation, this study aims to enhance this understanding that acts as an important building block for more complete understanding of aerosol-cloud-precipitation interactions in urban areas. Yes, aerosol physical and chemical processes and effects of clouds, convection, and turbulent mixing on aerosol distributions need to be explored for the complete understanding. However, this study does not focus on those processes and effects, and instead, aims to gain the understanding of effects of background aerosol itself on clouds and precipitation, since we believe that fulfilling this aim acts as an important first stepping stone to the complete understanding of aerosol-cloud-precipitation interactions in urban areas and understanding of the processes and effects in urban areas merits future study as a next stepping stone.

Although the background aerosol is prescribed, its properties are based on observation. Thus, although physical and chemical processes and the effects of cloud, convection, turbulence on the background aerosol are not considered, overall background aerosol properties including its spatial gradient are not that deviant from observed counterparts. This enables the good consistency in the locations of heavy precipitation between the simulation and observations, demonstrating that the simulations here are not that unrealistic despite the neglected aerosol processes and effects of clouds on the background aerosol.

In this study, the cloud system is over two sectors: the first sector is on the western side of the low-aerosol/high-aerosol boundary and the second sector is on the eastern side of the boundary. Then, we show that the sector on the western side experiences higher aerosol concentrations than that on the eastern side. Due to higher aerosol concentrations, there are lower autoconversion rate and thus a larger amount of cloud liquid as a source of evaporation, leading to higher evaporation rate in the sector on the western

side than in the sector on the east side. This higher evaporation rate in the sector on the western side is a key process to form the strong convergence field in the green rectangle. The sector of cloud system on the western side always experiences higher aerosol concentrations and produces higher evaporation rate than those on the eastern side until 19 LST when the strong convergence field in the green rectangle forms as shown in Figures 10 and 12. Basic cloud physics and dynamics (e.g., Rogers and Yau, 1991; Pruppacher and Klett, 1978) indicate that most of aerosol particles that are ingested into clouds are from around the surface just below those clouds. Hence, cloud cells of the cloud system on the western side are mostly affected by higher aerosol concentrations on the western side than those on the eastern side and this causes higher evaporation on the western side than on the eastern side. It is true that some of cloud cells on the western side can advect into the eastern side before they die. These cloud cells ingest higher (lower) aerosol concentration while they stay on the western (eastern) side; in other words, these cells ingest aerosol from various regions during their lifecycle as the reviewer phrases. However, these cloud cells produce lower (higher) autoconversion and higher (lower) evaporation rates, while they stay on the western (eastern) side. Hence, even these cells contribute to the higher evaporation rates on the western side and thus to the formation of the strong convergence line in the green rectangle, which is essential for the development of heavy precipitation as explained in the manuscript.

Considering the reviewer's comment here, the word "possibility" is replaced with "hypothesis" in Line 127 on p5.

Also, to reflect a point about the isolation of the effects of background aerosol in text, the following is added:

(LL291-298 on p10)

This assumption indicates that we do not consider the effects of clouds and associated convective and turbulent mixing on the properties of background aerosol. Also, above-explained prescription of those properties (e.g., number concentration, size distribution, and chemical composition) indicates that this study does not take aerosol physical and chemical processes into account. This enables the confident isolation of the sole effects of given background aerosol on clouds and precipitation in the Seoul area, which has not been understood well, by excluding those aerosol processes and cloud effects on background aerosol.

To remove the impression (pointed by the reviewer here) that "the spatial variability discussed here appear to be of much smaller scale than those investigated with the simulations with two different aerosol-concentration air masses over an area of about 100 x 100 km", we revised the corresponding text.

For the revision of text between line 117 and 123 in the old manuscript, we removed words like “district” and “city area”, which give the impression, as follows:

(LL130-139 on p5)

For example, cloud cells (in an MCS) sitting on a significant portion of a metropolitan area with a higher aerosol concentration can be invigorated more than those cells on the rest portion of the area with a lower aerosol concentration. This can lead to enhanced precipitation and possibly torrential rain at the portion with the higher aerosol concentration, while in the rest portion, there can be less precipitation. This creates an inhomogeneity of precipitation distributions that can accompany torrential rain in the specific portion of the area. A further increase in aerosol concentration in the portion with the higher aerosol concentration will further enhance precipitation and torrential rain there and thus create a greater inhomogeneity of precipitation distributions.

For the revision of text between line 730 and 734 in the old manuscript, we removed words like “traffic” and “sudden”, which give the impression, as follows:

(LL781-786 on p26)

For example, in a place such as a large-scale industrial complex within an urban area away from an urban boundary, there can be an increase in aerosol concentrations and thus high aerosol concentrations. These high aerosol concentrations can advect, as exemplified in the case adopted in this study, and a boundary between a place with low-aerosol concentrations and a place with high aerosol concentrations can vary spatiotemporally within the urban area.

References:

Rogers, R. R., and M. K. Yau, A short course in cloud physics, Pergamon Press, 293 pp, 1991.

Pruppacher, H. R. and J. D. Klett, Microphysics of Clouds and Precipitation, 714pp, D. Reidel, 1978.

3. Description of the model: The description of the model and the simulation set-up is scattered across section 2 and 3. In particular, many parts of section 3 detail the set-up of the model domains and the cloud microphysics instead of discussing the investigated case. The model description should be provided in one single section. The authors also say they developed a module to represent the spatial variability of

aerosol (p. 7, l. 193-194). It is not clear from the manuscript at this point what processes this entails. Please provide a better description of what processes are included.

The description of model, simulations and their set-up is now provided in one single section, which is Section 3.

The aerosol module simply interpolates the observed background aerosol properties such as PM_{10} at observation sites to model grid points and time steps. There are no other functions of the aerosol module other than this. The interpolated PM_{10} is used to calculate aerosol number concentration at each grid point and at each time step as explained in Section 3.2 by following assumptions on aerosol size distribution and composition as elaborated in Section 3.2.

More description of the aerosol module is now provided as follows:

(LL225-228 on p8)

For this, we develop an aerosol module that is able to represent the variability of aerosol properties. This aerosol module interpolates observed background aerosol properties such as aerosol mass (e.g., PM_{10}) at observation sites to model grid points and time steps. This aerosol module is now implemented to the ARW model.

3. Results: The analysis of the differences between the simulations, the physical mechanism driving these changes and the presented conclusions are not very convincing to me. While there are certainly differences in the convergence patterns between the runs, the physical mechanism is not clear. From the presented figures, I find it hard to believe that the difference in surface wind between the two air masses with different aerosol concentrations are a result of different latent cooling rates in the two areas, in particular as the convective systems are rather small compared to the extend of the wind field anomaly in the high-aerosol air mass during the initial stages of the simulation.

   As shown in Weisman and Klemp (1982) and Newton and Fankhauser (1975) that are well-known classic studies in the field of convection, the extension of the wind field anomaly, caused by evaporative cooling, is much greater than that of the area where cloud cells and associated evaporative cooling are located. It is well-known that the outflow from evaporation-driven downdrafts spreads out from cloud cells to surrounding much larger areas, leading to a situation where the extension of the wind field anomaly is much greater than that of the area where cloud

cells and associated evaporative cooling are located as in classic textbooks (e.g., Houze, 1993; Emanual, 1994). Consistent with those studies and textbooks, this study shows the extension of the wind field anomaly much greater than that of the area where cloud cells and associated evaporative cooling are located, particularly, in the part of the domain to the west of the strong convergence line in the green rectangle. In fact, the ratio of areas occupied by cloud cells to those occupied by the wind anomaly in those studies and textbooks is similar to that in this study.

References:

Emanuel, K., Atmospheric convection, Oxford University Press, 580 pp, 1994.

Houze, R. A., Cloud dynamics, Academic Press, 573 pp, 1993.

Newton, C. W., and J. C. Fankhauser, Movement and propagation of multicellular convective storms, Pageoph, 113, 747-764, 1975.

Weisman, M. L., J. B. Klemp, The dependence of Numerically Simulated Convective Storms on Vertical Wind Shear and Buoyancy, Mon. Wea. Rev., 110, 504-520, 1982.

Just looking at the wind fields in Fig. 9, it appears that there are significant differences in the wind field at the lateral boundaries. It would be interesting to investigate whether the changes in the wind field are due to cold pool formation in an upstream area of the domain 3. This is particularly important as the system at least in the initial and mature phase is located very close to the northern domain boundary (e.g. Fig. 7). Along these lines, it would be also important to assert that the meso-scale circulation patterns in the outer domains are similar in the additional sensitivity simulations the authors present. Is it possible that the large differences in the convergence and the lack of organization is related to changes in the meso-scale circulation in the outer domains?

Note that initial atmospheric fields including the temperature field, the wind field and circulation patterns over all of the three domains are identical between the control run and the low-aerosol run. Due to differences in aerosol spatial distribution and loading in Domain 3, after the initial time step and after clouds start to form, the differences in evaporative cooling and associated wind field in Domain 3 between the runs start to appear first; note that there are no differences in

aerosol spatial distributions and loading between the runs in Domain 1 and Domain 2. Then, these differences in Domain 3 induce differences in wind in the other two domains, considering two-way interactive triple-nested domains which are adopted by this study. Hence, differences in wind in Domain 1 and Domain 2 are results of those differences in Domain 3. These differences in Domain 2 in turn cause differences in wind around the boundary between Domain 2 and Domain 3. Hence, we want to emphasize that the differences in wind around the boundary are the subsequent result of the differences in aerosol and evaporative cooling in Domain 3 between the runs.

As seen in Figure 9 in the old manuscript, those differences (between the runs) in wind around the boundary (between Domain 2 and Domain 3) that corresponds to 0-100 km in the x direction and 70-180 km in the y direction of Domain 3 are amplified as wind moves southward and/or eastward from the boundary toward the inner part of Domain 3, since during this movement of the wind or outflow from the downdrafts, the wind or outflow is accelerated more due to more evaporation (and associated greater negative buoyancy) on the path of the movement in the control run than in the low-aerosol run. These amplified differences enable the large differences in the convergence field in the green rectangle between the runs. In particular, around the northern boundary that corresponds to 0-100 km in the x direction, there is stronger wind in the low-aerosol run than in the control run, which favors stronger convergence in the low-aerosol run in case the stronger wind in the low-aerosol run is maintained during the wind movement to the inner part of Domain 3. However, due to the amplification process during the wind movement, wind in the control run becomes stronger, leading to the stronger convergence in the rectangle in the control run. Here, we emphasize that the amplification, resulting in much stronger wind in the control run, occurs in Domain 3 BUT NOT in Domain 1 and Domain 2.

In summary, although there are differences in wind field or circulations in Domain 1 and Domain 2, these differences are caused by differences in aerosol and evaporative cooling between the runs in Doman 3. The differences in wind around the boundary between Domain 2 and Domain 3, which are caused by differences in Domain 2, are not able to explain the formation of the strong convergence field in the green rectangle. When those differences around the boundary are amplified via differences in evaporative cooling in Domain 3, the amplified differences eventually generate the large differences in the convergence field in the rectangle between the runs. This summary demonstrates that differences in aerosol and evaporative cooling in Domain 3

are the cause of differences in wind field in all of the three domains, and the differences in wind field in Domain 1 and Domain 2 are not able to explain the large differences in the strong convergence field in the rectangle between the runs. When the difference in wind in Domain 2, after wind in Domain 2 enters Domain 3, is amplified by differences in aerosol and evaporative cooling in Domain 3, the large difference in the convergence field in the rectangle is generated. This summary also demonstrates that without differences in aerosol and evaporative cooling in Domain 3, there is no formation of the strong convergence field in the rectangle. Stated differently, differences in aerosol and evaporative cooling in Domain 3 are a main cause of the large difference in the convergence field in the rectangle between the runs but not differences in circulations or wind fields in Domain 1 and Domain 2.

The following is added:

(LL568-572 on p19)

The outflow in the area with high-value aerosol concentrations accelerates, due to evaporation on its path, as it moves southeastwards from the northern and western boundaries of the domain. The outflow accelerates until it collides with surrounding air that has weaker horizontal movement in the area with low-value aerosol concentrations.

Another factor that is not at all mentioned are radiative effects of the aerosols that could impact the stability between the air masses with different aerosol concentrations. The authors say in the model description, that the aerosols interact with the radiative fluxes. These aspects need further investigation before any firm conclusions about the physical mechanism for the differences between the simulations can be drawn.

After aerosol particles are activated or cloud particles such as droplets are nucleated, aerosol-induced changes in the properties of cloud particles such as the effective size of droplets affect raditation in this study as described in text. However, before aerosol particles are activated, aerosol particles do not affect radiation, since observations do not show that strong radiation absorber such as black carbon is included in aerosol particles. Hence, in this study, we do not consider aerosol radiative effects that are the effects of aerosol particles on radiation before their activation.

The following is added:

(LL249-252 on p9)

Since the mixture includes chemical components that absorb solar radiation insignificantly as compared to strong radiation absorbers such as black carbon, we assume that the mixture does not absorb solar radiation and thus do not simulate the solar absorption of aerosol and attendant effects on stability.

Results: It is mentioned in the model description that ice- and mixed-phase processes are included in the microphysics module of the model. However, the discussion exclusively looks at warm-phase processes, i.e. using condensation/evaporation, autoconversion/accretion. If the simulations include mixed-phase processes, these need to be included in the analysis as well.

The following is added:

(LL496-499 on p17)

Other processes such as deposition and freezing produce the mass of solid hydrometeors and act as sources of precipitation, however, their contribution to precipitation is ~one order of magnitude smaller than that by condensation in the control run and the low-aerosol run. Hence, here, we zero in on condensation.

(LL551-554 on p19)

Sublimation and melting also enhance negative buoyancy, however, their contribution is ~one order of magnitude smaller than the contribution by cloud-liquid evaporation. Hence, here, we focus on cloud-liquid evaporation.

2 Specific comments

1. p. 4, l. 94: What is aerosol supposed to be most representative for?

Here, we meant that aerosol is included in a group of variables which have the high-degree spatial variability or whose values vary with time and space substantially. To remove confusion, the corresponding text is revised as follows:

(LL98-99 on p4)

Aerosol is also one of those variables which have large spatial variability.

2. p. 4, l. 105-108: The authors cite two studies to suggest that increasing aerosol concentrations can intensify deep convective clouds by enhanced latent heating due to freezing. This hypothesis has been discussed controversially in recent literature (e.g., van den Heever et al., 2006; Fan et al., 2009; Lebo and Seinfeld, 2011; Lebo, 2017) and this should be mentioned in the introduction.

The following is added:

(LL113-118 on p4)

Studies (e.g., van den Heever et al., 2006; Fan et al., 2009; Lebo and Seinfeld, 2011; Lebo, 2017) have shown that aerosol-induced invigoration of convection and enhancement of precipitation depend on competition between aerosol-induced increases in buoyancy and those in hydrometeor loading, and aerosol-induced increases in condensational heating and associated invigoration in the warm sector of a cloud system.

p. 5, l. 148: Please check this reference.

Checked and replaced with the following paper:

- Khain, A., A. Pokrovsky, D. Rosenfeld, U. Blahak, and A. Ryzhkov (2011), The role of CCN in precipitation and hail in a mid-latitude storm as seen in simulations using a spectral (bin) microphysics model in a 2D dynamic frame, *Atmos. Res.*, **99**, 129–146, doi:10.1016/j.atmosres.2010.09.015.

4. p. 9, l. 246: Do you mean the aerosol in the PBL does not vary vertically?

Yes. To clarify this, text is revised:

(LL282-285 on p10)

It is assumed that in the planetary boundary layer (PBL), background aerosol concentrations do not vary with height but above the PBL, background aerosol concentrations reduce exponentially with height.

5. p. 9, l. 255: Please chose a more meaningful title for this section. It would also be good to introduce all sensitivity simulations conducted in the paper here. In particular, the simulations with homogeneous aerosol concentrations, since these are the obvious test simulations the reader is expecting for addressing the outlined scientific questions.

We believe that the title should be simple and short, and should not be long and complicated. Hence, we replaced the old title with a simple and short title which is "3.3 Additional runs".

We introduced all sensitivity simulations in this section 3.3 as follows:

(LL328-342 on p11-12)

In addition to the control run and the low-aerosol run, there are more simulations that are performed to better understand the effect of aerosol on precipitation here. To isolate the effects of aerosol concentrations on precipitation from those of aerosol spatial variability or vice versa, the control run and the low-aerosol run are repeated with homogeneous spatial distributions of aerosol. These homogeneous spatial distributions mean that there is no contrast in aerosol number concentrations between the western part of the domain and the eastern part, and aerosol number concentrations do not vary over the domain. The repeated simulations are referred to as the control-homoge run and the low-aerosol-homoge run. The analyses of model results below indicate that differences in precipitation between the control run and the low-aerosol run are closely linked to cloud-liquid evaporative cooling and to elucidate this linkage, the control run and the low-aerosol run are repeated again by turning off cooling from cloud-liquid evaporation. These repeated simulations are referred to as the control-noevp run and the low-aerosol-noevp run. While a detailed description of those repeated simulations is given in Section 4.3, a brief description is given in Table 1.

6. p. 9, l. 257: The aerosol field consist of two air masses with two different aerosol concentrations and a relatively small transition zone between the two. I would not call this is "high-degree spatial inhomogeneity". Please avoid using this term. However, I agree that the aerosol variability investigated here is larger than in most numerical studies, which do nor represent spatial aerosol variability.

The term is replaced with "large spatial variability"

7. p. 9, l. 269: It is claimed that the effects of inhomogeneity and number concentration can be investigated. However, it is not possible discriminate the impact of two changes based on just the two simulations, which have been introduced in the manuscript up to this point.

Following the comment #5 above, we introduced additional simulations for the discrimination in Section 3.3.

8. p. 10, l. 303: Please specify whether these are surface precipitation observations or derived from radar data.

Precipitation is directly measured by rain gauges that are parts of AWS. To clarify this, text is revised as follows:

(LL370-371 on p13)

Here, observed precipitation is obtained from measurement by rain gauges that are parts of the automatic weather system (AWS) at the surface.

9. p. 11, l. 313: Have you interpolated the 3km observational data to the 500m model data. The linear interpolation does not represent the correct frequency distribution at higher resolution. A less problematic approach would be to coarse-grain the model data to the resolution of the observational data.

Based on this comment, we checked the validity of the interpolation of observational data to model data by performing the suggested interpolation of model data to observation points. However, this suggested interpolation gives us the same conclusion as the previous interpolation which is described in Section 4.1.2. Hence, we let the previous interpolation stay in the manuscript.

10. e.g. p. 15, l. 427/428: The authors refer at various points to an “extension” or “movement” of the convergence field. I think they refer to changes in the spatial extend or location of regions with high convergence. The formulation should be altered accordingly.

Following comments by the other reviewer, Section 4.2.1 is simplified and during this process of simplification, text including extension and movement of the convergence field is removed.

11. p. 18, l. 520: Is the different location of the convergence line in the two simulations taken into account for the calculation of the mean values? And its eastward propagation?

For Figures 12a and 12b, the average is performed over the period between 17 and 19 LST. The strong convergence field and associated heavy precipitation, in the area surrounded by the green rectangle, start

to appear up when time reaches around 19 LST in both of the runs. However, during most of the period between 17 and 19 LST, the strong convergence field and heavy precipitation are absent and thus, the area which can be marked by the green rectangle is not identified. In other words, during most of the period between 17 and 19 LST, the green rectangle is not identified and when time reaches around 19 LST, the rectangle starts to be identified. We are simply interested in differences in evaporation between areas to the east of the rectangle and those to the west before 19 LST, more specifically, between 17 LST and 19 LST without needing to consider the eastward propagation of the green rectangle due to its absence between 17 LST and 19 LST; here, we just want to say that although the rectangle is absent between 17 LST and 19 LST, we can apply the locations of the rectangle at 19 LST to the period before 19 LST as a process of identifying those areas to the east and those areas to the west before 19 LST. This interest is caused by the fact that those differences in evaporation before 19 LST affect differences in downdrafts and its outflow (between areas to the east of the rectangle and those to the west) that are essential for the formation of the strong convergence line in the green rectangle around 19 LST.

To indicate that the green rectangle starts to form around 19:00 LST, the following is added:

(LL429-430 on p15)

Since heavy precipitation starts to form around 19:00 LST, the green rectangle starts to be identified around 19:00 LST.

Yes, it is true that the location of the convergence line or the green rectangle is slightly different between the runs at 19 LST as shown in Figures 8, 10, and 11 and this was reflected for the calculation of differences in evaporation between areas to the east of the rectangle and those to the west for the period between 17 LST and 19 LST. However, in the old manuscript, the reflection was not indicated. To correct this, the following is added:

(LL526-538 on p18)

For the calculation of the averaged values in Figure 12, the area to the west (east) of the strong convergence field is set to include all parts of the north-south direction, which is the y-direction, and the vertical domains but a portion of the east-west direction domain, which is the x-direction domain that extends from the western boundary of Domain 3 to 90 km where the western boundary of the green rectangle at 19:00 LST is located (from 110 km where the eastern boundary of the green rectangle at 19:00 LST is located to the eastern boundary of Domain 3) in Domain 3 for the control run. For the low-aerosol run, the area to the west (east) of the strong convergence field is identical to that in the control run

except for the fact that the area includes a portion of the x-direction domain that extends from the western boundary of Domain 3 to 70 km where the western boundary of the green rectangle at 19:00 LST is located (from 90 km where the eastern boundary of the green rectangle at 19:00 LST is located to the eastern boundary of Domain 3) in Domain 3.

12. p. 20, l. 586: What is the motivation for not switching of latent cooling from rain evaporation? This is usually considered the most important for cold-pool formation and the interaction of deep convective systems with boundary-layer dynamics.

It is known that downdrafts are generally initiated by the loading of raindrops that drags down air parcels (Houze, 1993). However, once downdrafts are initiated or once air parcels (having both cloud liquid (or droplets) and rain (or raindrops)) start to move downward, the speed of air parcels moving down or the speed of downdrafts is strongly controlled by the negative buoyancy and the negative buoyancy is mostly provided by evaporation of liquid particles in those air parcels (Houze, 1993 and Bluestein, 1993). The terminal velocity of droplets is negligible as compared to that of rain drops and thus it can be assumed that droplets within air parcels move together with air parcels and thus droplets within air parcels remain in those parcels as those parcels move downward as downdraft entities or move upward as updraft entities; in general, in microphysics parameterizations, cloud liquid or droplets are assumed to have no or negligible terminal velocity and thus to move with air parcels or wind. In this study, rain evaporation and associated cooling (as a source of negative buoyancy) are smaller over the west part of the domain than over the east part of the domain as seen in Figure 12a, while cloud-liquid evaporation and associated cooling (as another source of negative buoyancy) are greater over the west part than over the east part in air parcels. Hence, the greater negative buoyancy and the associated greater speed of air parcels moving downward or the greater speed of downdrafts over the west part than over the east part are induced by the greater cloud-liquid evaporation but not by the smaller rain evaporation in those air parcels over the west part than over the east part.

To clarify the role of cloud-liquid evaporation against that of rain evaporation, we added rain evaporation in Figure 12a and associated text. Also, the following is added to give a more explanation of the effect of cloud-liquid evaporation on downdrafts:

(LL557-564 on p19)

Previous studies have shown that aerosol-induced increases in cloud-liquid evaporation are closely linked to the enhancement of the intensity of downdrafts (Lee et al., 2008a, b; Lee et al., 2013; Lee, 2017). Cloud liquid or droplets in downdrafts move together with downdrafts, thus, when downdrafts descend,

cloud liquid descends while being included in downdrafts. Cloud liquid in the descending downdrafts evaporates. More evaporation of cloud liquid provides greater negative buoyancy to downdrafts so that they accelerate more (Byers and Braham, 1949; Grenci and Nese, 2001).

References:

Byers, H. R., and Braham, R. R., The thunderstorm, U. S. Weather Bur., Washington, D. C., 287 pp, 1949.

Grenci, L. M., and Nese, J. M., A world of weather: fundamentals of meteorology: a text/ laboratory manual, Kendall/Hunt Publishing Company, 2001

13. Figure 1: Can you include the topography in this plot. This would be interesting for readers not very familiar with the geographic context.

Done.

14. Figure 5 and 6: Can you include all the results from all sensitivity experiments in these plots?

Done.

15. Figure 7: I find the contour plots extremely hard to read, especially the different contours for the precipitation rate. Would it be possible to use filled contours to show the precipitation rates?

Filled contours are now used for precipitation and shown in Figures 8, 10, and 11.

16. Figure 11: It would be interesting to show the evolution of the low-level wind field in these simulations and for earlier times as well.

Done.

3 Technical corrections

There are numerous places in the manuscript, where the language is quite awkward and reformulation of the sentences should be considered. In particular, please check the use of articles. A none exhaustive list is provided:

• The authors use phrases like ”frequency or occurrence” in many places (e.g. page 3, line 59; page 9, line 264/265; etc). These ”or”-statements should be removed and just one term be used.

Done.

• p. 4, l. 101: “Collision and collection are”

Done.

• p. 5, l. 123: “A further increase in aerosol loading in the district ...”

Done.

• p. 5, l. 125: “... create a greater inhomogeneity ...”

Done.

• p. 5, l. 131: “ ... select a MCS over ...”

Done.

• p. 7, l. 183: “ ... the large-scale environment ...”

Done.

• p. 7, l. 186: “... assumes horizontally homogeneous aerosol properties ... ”’

Done.

• p. 7, l. 191: “... assumption of homogeneity and ... spatio-temporal inhomogeneity ...”

Done.

• p. 7, l. 193: “... able to represent the inhomogeneity ...”

Done.

• p. 7, l. 197: “... with about 1 km distance ...”

Done.

• p. 7, l. 200: “ ... size distributions at those sites ...”

Done.

• p. 7, l. 210: “... follow a tri-modal ...”

Done.

• p. 8, l. 218: “... and aerosol particles are assumed to be internally mixed.”

Done.

• p. 8, l. 230: “... above, precipitation is ...”

Done.

• p. 10, l. 279: “... has ”low” inhomogeneity ...”

Done.

• p. 10, l. 302: “... simulations perform reasonably ...”

Done.

• p. 11, l. 316: “... the observed frequency distribution is consistent with the ...”

Done.

• p. 12, l. 340: “... initial stages of the precipitating system ...”

Done.

• p. 12, l. 354f: Please explicitly state the meaning of these lines again.

Done.

• p. 12, l. 360: “By 20:00 LTS the maximum ...”

Done.

• p. 13, l. 375: “ ... Figure 7e for easier comparison. This ...”

Done.

• p. 13, l. 378: “The system propagates eastwards after 20:00 LST ...”

Done.

• p. 15, l. 444: "... the associated larger intensification ..."

The paragraph including this sentence is removed by following a comment by a reviewer.

• p. 15, l. 456: Can you please rephrase this sentence, its meaning is unclear to me in its current form.

The paragraph including this sentence is removed by following a comment by a reviewer.

• p. 17, l. 512f: "... there is a larger horizontal wind-speed than in ..."

Done.

• p. 21, l. 624: "... vice versa. For this purpose, ..."

Done.

References

Fan, J., T. Yuan, J. M. Comstock, S. Ghan, A. Khain, L. R. Leung, Z. Li, V. J. Martins, and M. Ovchinnikov, 2009: Dominant role by vertical wind shear in regulating aerosol effects on deep convective clouds. J. Geophys. Res. Atmos., 114, D22206, doi:10.1029/2009JD012352.

Lebo, Z., 2017: A numerical investigation of the potential effects of aerosol-induced warming and updraft width and slope on updraft intensity in deep convective clouds. J. Atmos. Sci., doi:10.1175/JAS-D-16-0368.1.

Lebo, Z. J. and J. H. Seinfeld, 2011: Theoretical basis for convective invigoration due to increased aerosol concentration. Atmos. Chem. Phys., 11, 5407–5429, doi:10.5194/acp-11-5407-2011.

van den Heever, S. C., G. G. Carrió, W. R. Cotton, P. J. DeMott, and A. J. Prenni, 2006: Impacts of nucleating aerosol on florida storms. part I: Mesoscale simulations. J. Atmos. Sci., 63, 1752–1775, doi:10.1175/JAS3713.1.

First of all, we appreciate the reviewer's comments and suggestions. In response to the reviewer's comments, we have made relevant revisions to the manuscript. Listed below are our answers and the changes made to the manuscript according to the questions and suggestions given by the reviewer. Each comment of the reviewer (in black) is listed and followed by our responses (in blue).

Review of "Aerosol as a potential factor to control the increasing torrential rain events in urban areas over the last decades" submitted to ACP for publication by Lee et al.

The authors examine the roles played by aerosol concentration and spatial distribution in torrential rain that occurred in Seoul, using cloud-system resolving model simulations. The model results show that the inhomogeneity of the spatial distribution of aerosol concentrations or loading causes the inhomogeneity of the spatial distribution of evaporative cooling and the intensity of associated outflow around the surface. This inhomogeneity generates a strong convergence field in which torrential rain forms. The effects of the increases in the inhomogeneity play a much more important role in the increases in torrential rain than the much-studied effects of the increases in aerosol loading.

The study provides new understanding about aerosol effects on convection and precipitation over large cities, which warrants a publication in ACP. However, many clarifications are needed before the paper can be accepted as shown below, particularly in the introduction, model description and the model results on the section of convergence. In addition, if aerosol radiative effects are included (it seems to be that way, but not very sure), then the results shown are not only the indirect effects. When you change aerosol concentration or inhomogeneity, aerosol radiative effects also change, and this impact could be more significant. The could impact the standpoint of your analysis in Section 4 (currently, your standpoint is purely from aerosol indirect effect).

Section 1,

1. Line 80-86, The description here mixes the cloud cell dynamics with synoptic-scale dynamics. It is true that synoptic-scale dynamics may be homogenous for MCS. However, the convective cells are affected by many small-scale dynamics such as cold pool, rear-inflow, wind shear, vortex, etc. Those small-scale cloud dynamical processes are generally inhomogeneous even with the same aerosol loading everywhere because they are complexly impacted by small-scale environment such as land-surface, microphysics, etc. Aerosol inhomogeneity could only be one of these factors. Therefore, the description here needs to be rewritten.

> We agree that the small-scale dynamics and small-scale environment, mentioned by the reviewer here, are factors which disrupt the synoptic-forcing-induced homogeneity of the MCS in urban areas (as we phrased in text). For this study, among those factors, we focus on aerosol. Text is revised to reflect these reviewer' and authors' points as follows:

(LL91-101 on p4)

The highly inhomogeneous distribution of precipitation means that there are highly inhomogeneous variables, processes and forcings which disrupt the synoptic-forcing-induced homogeneity of MCSs in urban areas. Some of those forcings are mesoscale forcings that show mesoscale variability and, for example, are related to phenomena such as sea-breeze fronts and lake breezes. In particular, in urban areas, due to strong heat fluxes at the surface, there is the urban heat island (UHI) effect as another example of those phenomena. Examples of those variables and processes are cold pool, rear inflow, wind shear, and mesoscale vorticity. Aerosol is also one of those variables which have large spatial variability. In particular, urban aerosol particles are produced by randomly distributed sources (e.g., traffic), which enables aerosol to have large variability in urban areas.

(LL136-144 on p5)

A further increase in aerosol concentration in the portion with the higher aerosol concentration will further enhance precipitation and torrential rain there and thus create a greater inhomogeneity of precipitation distributions. Motivated by the hypothesis and associated argument here, among the forcings, processes and variables which have spatial variability, this study focuses on aerosol. To examine aerosol effects on clouds and precipitation, numerical simulations are performed by using a cloud-system resolving model (CSRM) that resolves cloud-scale microphysical and dynamic processes and simulates the effect of the variability and loading of aerosol on precipitation.

2. Line 92-94, similar comment as above. The inhomogeneity of the convective cell and precipitation occurs everywhere, not only just over urban area. Many other factors could contribute to the inhomogeneity. For the urban area, there is effect of urban heat, which is so relevant and should be discussed in the introduction.

See our response to the comment 1. The urban heat or the urban heat island (UHI) effect is included in introduction as shown in our response to the comment 1. Also, the UHI effect is discussed in “summary and conclusion”.

3. Line 106-108, Are you talking about observed studies here? If so, then need to be clear about it. If not, you should cite the symbolic papers illustrating the invigoration through enhanced latent heat induced by freezing such as Khain et al. 2005 and Rosenfeld et al. 2008.

Those symbolic papers are now included.

4. The description about literature studies in aerosol indirect effects on convective clouds are

one-sided. Many studies showed that the enhanced or suppressed precipitation by aerosols could be very dependent on RH, wind shear, CAPE, etc., which should be clearly delivered to readers.

The following is added:

(LL118-121 on p4-5)

Other studies (e.g., Khain et al., 2008; Lee et al., 2008b; Fan et al., 2009) have shown that the invigoration-related enhancement of precipitation also depends on environmental conditions that are represented by wind shear, relative humidity, and instability.

Section 3,

1. Section 3.1, first paragraph, what are the domain sizes? Where is Seoul in Domain 3?

The Seoul boundary is marked in Figure 2. Seoul city itself occupies a portion of Domain 3, however, in this study, the Seoul area means the conurbation area or the metropolitan area that is composed of Seoul and highly populated cities around Seoul in Domain 3. To clarify this, the following is added:

(LL201-205 on p7)

The Seoul area is a conurbation area that centers in Seoul and includes Seoul and surrounding highly populated cities. Hence, the Seoul area is composed of multiple cities whose total population is ~twenty five millions. The boundary of Seoul, which has the largest population among those cities, is marked by a dotted line in Figure 2.

The following is added to indicate the domain sizes:

(LL198-201 on p7)

The length of Domain 3 in the east-west direction is 220 km, while the length in the north-south direction is 180 km. The lengths of Domain 2 and Domain 3 in the east-west direction are 390 and 990 km, respectively, and those in the north-south direction are 350 and 1100 km, respectively.

2. Line 165, Domain 1 is 4.5 km. Does the cumulus parameterization work for this resolution?

   We used Kain and Fritsch's cumulus parameterization scheme. According to Gilliland and Rowe (2007), the use of this scheme at a resolution similar to 4.5 km does not affect the quality of the simulation of convective cells and instead, this use improves the

quality of the simulation of some features of those cells. Hence, we believe that the use works reasonably well.

The following is added:

(LL211-213 on p7-8)

Here, we use a cumulus parameterization scheme that was developed by Kain and Fritsch (1990 and 1993). This scheme is shown to work reasonably well for resolutions that are similar to what is used for Domain 1 (Gilliland and Rowe, 2007).

3. About the RRTMG scheme you used, did you use the effective radius calculated from microphysics in the radiation calculation?

The following is added:

(LL180-183 on p6-7)

The effective sizes of hydrometeors are calculated in a microphysics scheme that is adopted by this study and the calculated sizes are transferred to the RRTMG. Then, the effects of the effective sizes of hydrometeors on radiation are calculated in the RRTMG.

4. Line 192: need some details about the aerosol module you developed. What was included in the module and is there any reference? Is aerosol formation excluded? If so, how are aerosol properties (SD, composition, vertical distribution) specified? How are the aerosol optical properties calculated? Is aerosol module similar to the idea used in Fan J. et al. 2008, JGR? If so, providing references would help readers understand better about what the aerosol module is.

The aerosol module simply interpolates the observed background aerosol properties such as PM_{10} at observation sites to model grid points and time steps. There are no other functions of the aerosol module other than this. The interpolated PM_{10} is used to calculate aerosol number concentration at each grid point and at each time step as explained in Section 3.2 by following assumptions on aerosol size distribution and composition as elaborated in Section 3.2.

To better describe aerosol module, the following is added:

(LL226-228 on p8)

This aerosol module interpolates observed background aerosol properties such as aerosol mass (e.g., PM_{10}) at observation sites to model grid points and time steps. This aerosol module is now implemented to the ARW model.

The assumptions on aerosol size distribution and composition or specified aerosol size distribution and composition are described in Section 3.2. The assumed vertical distribution of aerosol is also described in Section 3.2. In this study, aerosol radiative properties, which are associated with aerosol optical properties, are not considered. To clarify this, the following is added:

(LL249-252 on p9)

Since the mixture includes chemical components that absorb solar radiation insignificantly as compared to strong radiation absorbers such as black carbon, we assume that the mixture does not absorb solar radiation and thus do not simulate the solar absorption of aerosol and attendant effects on stability.

5. Line 222-223, how did you convert PM10 to aerosol number concentration? Theoretically you can not do this since PM10 is only contributed by the very large aerosol particles. Do you have any reference for what you did here?

We calculate aerosol mass for each size bin of the size distribution up to 10 micron in Figure 3 based on assumptions of aerosol chemical composition and associated aerosol particle density; we just want to remind that the assumed size distribution and aerosol chemical composition are obtained based on the analysis of the AERONET observation.

In the size distribution in Figure 3, which is obtained by the AERONET observation, we know the aerosol number for each size bin and this aerosol number is multiplied by the particle density, which is calculated based on the assumed aerosol chemical composition, to obtain the aerosol mass for each size bin. Then, we sum up the aerosol mass for each size bin over all bins up to 10 micron in the size distribution to obtain PM10 which is referred to as PM10_standard. At each grid point and at each time step in the model domain and over the simulation period, we have an observed PM10 varying from one grid point to the other and with time, referred to as PM10_grid. We calculate the ratio which is "PM10_grid/PM10_standard". To obtain the size distribution at each grid point and at each time step, based on the assumption that the size distribution of background aerosol at all grid points and time steps has the size distribution parameters or the shape of distribution that is identical to that in Figure 3, the aerosol number for each size bin of the size distribution of aerosol number in Figure 3 is multiplied by this ratio. After this multiplication, the new aerosol number, which is the aerosol number multiplied by the ratio, in each bin is summed up over size bins up to 10 micron to obtain total aerosol number concentration at each grid point and at each time step. Note that after this multiplication, if we sum up aerosol mass (corresponding to the new aerosol number) over size bins up to 10 micron, the sum is equal to PM10_grid at each grid point and at each time step.

As shown in Figure 6.3 in Rogers and Yau (1989; the third edition), it is true that large particles make the large contribution to total aerosol mass. However, it does not prevent the conversion between mass (or PM10) and number as described in Tittarelli et al. (2008). In addition,

Tittarelli et al. (2008) showed that small particles smaller than 1 micron contribute to the total aerosol mass or PM10 as much as those particles greater than 1 micron for their selected cases. The observed size distribution of aerosol particle mass by AERONET for the case here shows the large contribution of large particles to total aerosol mass or PM10. However, when the size distribution of aerosol particle mass is converted to that of aerosol number, most of contributions to total aerosol number are made by small aerosol particles whose size is smaller than 1 micron as exemplified by Figure 3. This point can be seen in comparisons between the first panel and the third panel in Figure 6.3 in Rogers and Yau (1989; the third edition).

To clarify assumption used to convert PM10 to aerosol number concentration, the following is added:

(LL254-257 on p9)

Stated differently, it is assumed that the size distribution of background aerosol at all grid points and time steps has size distribution parameters or the shape of distribution that is identical to that in Figure 3.

Reference:

Rogers, R. R., and M. K. Yau, A short course in cloud physics, Pergamon Press, 293 pp, 1989.

Tittarelli, A., Borgini A., Bertoldi, M., et al., Estimation of particle mass concentration in ambient air using a particle counter, Atmos. env., 42, 8543-8548, 2008.

6. Line 237-238, the aerosol generation is not included in the SBM released in WRF. The reference Fan et al. 2009 shown here indeed had it for that study, but it was not included in the WRF releases. Did you make your own code to do this or you assumed this process was included in the released version?

We checked the code and found that the aerosol generation has not been included yet. Text is revised accordingly.

7. Description of model simulations and Table 1 are confusing currently. Need clear description about how the aerosol concentration and inhomogeneity are changed, respectively, from one to other simulations. For example, in Line 279-280, “The repeated simulation has the “low” inhomogeneity and concentrations of “aerosol” as compared to the control run and thus is referred to as the low-aerosol run”, if both aerosol number and inhomogeneity are changed as described here, then how do you distinguish the effect by changing aerosol number from changing aerosol inhomogeneity? What are the other simulations you ran to help you distinguish? As I read along, I found much of the description is at the different result parts. So, the description should be moved to here to help people clearly understand the purpose of the simulations and how the simulations were set up.

To clarify additional simulations for the distinguishment between the effect of aerosol number and that of inhomogeneity, and those additional simulations with evaporative cooling off, the following is added in Section 3.3:

(LL329-342 on p11-12)

To isolate the effects of aerosol concentrations on precipitation from those of aerosol spatial variability or vice versa, the control run and the low-aerosol run are repeated with homogeneous spatial distributions of aerosol. These homogeneous spatial distributions mean that there is no contrast in aerosol number concentrations between the western part of the domain and the eastern part, and aerosol number concentrations do not vary over the domain. The repeated simulations are referred to as the control-homoge run and the low-aerosol-homoge run. The analyses of model results below indicate that differences in precipitation between the control run and the low-aerosol run are closely linked to cloud-liquid evaporative cooling and to elucidate this linkage, the control run and the low-aerosol run are repeated again by turning off cooling from cloud-liquid evaporation. These repeated simulations are referred to as the control-noevp run and the low-aerosol-noevp run. While a detailed description of those repeated simulations is given in Section 4.3, a brief description is given in Table 1.

We just give a brief overview of the repeated simulations in Section 3.3 as above and their more detailed description is given in Section 4.3. Since Section 4.3, which contains results from those repeated simulations, appears up much later than Section 3.3 and thus, when readers reach Section 4.3 to read results from the repeated simulations, readers may not recognize the nature of those repeated runs at first sight without their description in Section 4.3. This can disable readers from understanding the results well. Hence, we believe that giving the description of the runs and their results together in Section 4.3 will enable readers to understand the results with efficiency. With this thought, we put the description in Section 4.3 as well as Section 3.3. In addition, the detailed simulation setup for the repeated runs is based on the analyses of results from the standard runs (i.e., the control run and the low-aerosol run) which are described in Sections 4.1 and 4.2. Hence, we believe that giving the detailed description of the setup in Section 4.3 after explaining those analyses in Sections 4.1 and 4.2 makes the description make more sense.

In addition, Table 1, the two columns “Contrast in aerosol spatial distribution” (Column 2) and “The homogeneous aerosol distribution” (Column 4) mean the similar thing to me. The content in Column 2 “reduced by a factor of 2”, does not make sense if it is for “Contrast in aerosol spatial distribution”. Did you mean “Contrast in aerosol number concentration”?

Yes, in column 2, we agree that “contrast in aerosol number concentration” is a better expression than “contrast in aerosol spatial distribution”. Table 1 is revised accordingly. Also, to

reflect the other points raised by the reviewer here, Table 1 is further revised. See Table 1 for details.

8. It is not clear if you excluded aerosol radiative effect or not? If so, please be very clear about it. If not, then the effects we see are not only the indirect effects. When you change aerosol concentration or inhomogeneity, aerosol radiative effects also change, and this impact could be more significant. The could impact your analysis in Section 4.

Aerosol radiative effect is excluded. To clarify this, the following is added:

(LL249-252 on p9)

Since the mixture includes chemical components that absorb solar radiation insignificantly as compared to strong radiation absorbers such as black carbon, we assume that the mixture does not absorb solar radiation and thus do not simulate the solar absorption of aerosol and attendant effects on stability.

Section 4,

1. Sections 4.1.1 and 4.1.2, the comparison of precipitation with observations does not seem to be fair since there is a significant fraction of the domain over ocean where no measurements are available. In addition, how about the evaluation of meteorological fields with observations? There should be a lot sounding measurements over Seoul.

We just want to confirm that for the comparison of precipitation between observation and the simulation over Domain 3, we extrapolated the land observation to ocean.

Only ~20% of Domain 3 is occupied by ocean and thus, we believe that ocean does not occupy a significant portion of Domain 3. Hence, we think that ocean does not affect the conclusions from the comparison between observation and the simulation significantly. When we performed the comparison between observation and the simulation only over land area (without the extrapolation of land observation to ocean), this comparison gives us the same conclusions that are already given in the old manuscript. Hence, due to the small portion of ocean area, inclusion of ocean through the extrapolation in the comparison does not affect the qualitative nature of conclusions from it.

There is a good consistency between simulated meteorological fields and observed counterparts as shown in Figure5.

The following is added:

(LL354-364 on p12)

Figure 5 shows the observed and simulated vertical profiles of potential temperature, water-vapor mass density, u-wind speed, and v-wind speed which represent meteorological fields. Radiosonde data as observation data are averaged over observation sites in the domain and the simulation period, while simulated meteorological fields are averaged over the domain and the simulation period to obtain the profiles. Positive (negative) u-wind speed represents eastward (westward) wind speed, while positive (negative) v-wind speed represents northward (southward) wind speed. Comparisons between the observed profiles and the simulated counterparts show that overall differences between them are within ~ 10% of observed values. Hence, with confidence, it can be considered that the simulation of meteorological fields is performed reasonably well.

2. It seems that there is an inconsistency between Figure 5 and Figure 6a for the differences between low aerosol and control runs. Figure 5 does not show that the precipitation in low-aerosol case has significantly smaller precipitation. However, Figure 6a suggest the rain should be much lower in that case because the total precipitation is mainly determined by the moderate and heavy rain rates.

We checked the program code calculating the precipitation frequency and found no errors in it.

For the moderate rain between ~10 and 60 mm hr^{-1}, the frequency is higher in the low-aerosol than in the control run. For the weak rain below 10 mm hr^{-1}, the frequency is also slightly higher in the low-aerosol run. Note that the frequency range is ~10^3 to ~10^5 for the moderate and weak precipitation and the range is ~1 to ~10^3 for the heavy precipitation. Hence, overall, the frequency range is ~two orders of magnitude greater for the moderate and weak precipitation than for the heavy precipitation. Due to the use of the log scale, it appears that there are the largest differences for the heavy precipitation and they govern the overall differences between the runs. However, although it appears that the differences for the weak and moderate precipitation are relatively much smaller (due to the use of the log scale), due to the frequency range which is much greater for the weak and moderate precipitation than for the heavy precipitation, the seemingly smaller differences for the weak and moderate precipitation can offset the seemingly larger differences for the heavy precipitation, leading to the similar total precipitation amount between the runs.

3. Line 338-341, Figure 7, the figure caption is very long and confusing. The light blue contours represent precipitation rates, but they are hard to see and the values for contour line are not clearly shown or described. Also, there could be timing shift between the convective developments in two simulations so comparison between the two simulations at a particular time may not be meaningful.

Precipitation rates are shown in new figures which are Figures 8, 10, and 11, and precipitation rates are represented by filled contours. Accordingly, the figure caption is simplified.

Yes, it is true that there can be timing shift in the convective development between the runs. However, as implied in Figure 6 that shows the similar precipitation temporal evolution between the runs, overall convection temporal evolution is similar between the runs. Convection and associated precipitation start to develop and reach their peak at a similar time before 00 LST on July 28th and then they decay after 00 LST on July 28th in both of the runs. Hence, we believe that it is not that unreasonable to say that the convection temporal development is similar between the runs. This similar development between the runs can be explained by the fact that identical synoptic-scale environment and its evolution are applied to both of the runs, and this synoptic environment and its evolution control the overall evolution of the system and associated convection.

4. Figure 8, I guess the plots are for the control run? I did not find such information in the figure caption or text. I had a trouble to understand what was plotted. Compared with Figure 7c and e, Figure 8a and 8b correspondingly have the same spatial domain for the same time, but I do not understand why the blue line and the green boxes are totally different.

We want to emphasize that the blue line is NOT from the control run BUT from observation as stated in the figure caption. We just wanted to compare the location of the green rectangle with the location of the observed heavy precipitation.

Yes, Figure 8 in the old manuscript or Figure 9 in the new manuscript is for the control run and this is now indicated in the figure caption. We double-compared the locations of the green rectangles at 19 and 20 LST in Figure 9 to those in Figure 8 (in the new manuscript) and found that the locations in Figure 9 are identical to those in Figure 8. Due to differences in the number of figure panels between different pages of the manuscript, panels are scaled differently between those pages and this makes the locations appear different between pages.

5. Please mark the city boundary or the boundary between the high/low boundaries in Figures 7-9.

The high/low boundaries are marked.

6. Section 4.2.1, the long text of the first 4 paragraphs can be simplified with just a few sentences since most of the description here is just the basic text book knowledge about the relationship of convergence, condensation, and precipitation. What's interesting here should be just the differences between the control and low-aerosol runs. Then the text that follows it should be explaining the reasons for the differences in convergence, condensation, and precipitation. The long text in this section makes readers very hard to get what the main points are.

The first 4 paragraphs are simplified into 1 paragraph. See text for more details.

7. Line 670-675, very long sentence and the meaning does not make sense based on the results shown. For example, “the absence of the strong convergence field in the control-homoge run results in the situation where the increase in the frequency of heavy precipitation in the control-homoge run” is opposite to the results shown above

As explained in text before, the strong convergence field, which is distinguishable from any other lines as shown in the green rectangles, in the control run plays an important role in much more heavy precipitation events in the control run than in the low-aerosol run. However, in the control-homoge run, there is no such strong convergence field, due to homogeneous aerosol spatial distributions, and so, there are insignificant differences in the frequency of heavy precipitation between the control-homoge run and the low-aerosol-homoge run, although there is a larger frequency of heavy precipitation in the control-homoge run than in the low-aerosol-homoge run. To clarify this and make the sentence clear, the corresponding text is revised as follows:

(LL715-725 on p24)

There is the larger frequency of heavy precipitation in the control-homoge run than in the low-aerosol-homoge run (Figure 7c). However, as mentioned above, there is no strong convergence field which is distinguishable from any other lines in the control-homoge run as seen in Figure 13c. Associated with this, differences in the frequency of heavy precipitation between the control-homoge run and the low-aerosol-homoge run are much smaller than those between the control run and the low-aerosol run particularly during the period between 19:00 LST and 23:00 LST, as seen in Figures 7i and 7l. This results in a situation where differences in the frequency of heavy precipitation between the control-homoge run and the low-aerosol-homoge run are, on average, just ~15 % of those between the control run and the low-aerosol run for the whole simulation period (Figure 7c).

Aerosol as a potential factor to control the increasing torrential rain events in urban areas over the last decades

Seoung Soo Lee[1], Zhanqing Li[1], Yong-Sang Choi[2], and Chang-Hoon Jung[3]

[1]Earth System Science Interdisciplinary Center, University of Maryland, Maryland

[2]Department of Environmental Science and Engineering, Ewha Womans University, Seoul, South Korea

[3]Department of Health Management, Kyungin Women's University, Incheon, South Korea

Corresponding author: Seoung Soo Lee
Office: (303) 497-6615
Cell: (609) 375-6685
Fax: (303) 497-5318
E-mail: cumulss@gmail.com, slee1247@umd.edu

Abstract

This study examines the role played by aerosol in torrential rain that occurred in the Seoul area, which is a conurbation area where urbanization has been rapid in the last few decades, using cloud-system resolving model (CSRM) simulations. The model results show that the spatial variability of aerosol concentrations causes the inhomogeneity of the spatial distribution of evaporative cooling and the intensity of associated outflow around the surface. This inhomogeneity generates a strong convergence field in which torrential rain forms. With the increases in the variability of aerosol concentrations, the occurrence of torrential rain increases. This study finds that the effects of the increases in the variability play a much more important role in the increases in torrential rain than the much-studied effects of the increases in aerosol loading. Results in this study demonstrate that for a better understanding of extreme weather events such as torrential rain in urban areas, not only changing aerosol loading but also changing aerosol spatial distribution since industrialization should be considered in aerosol-precipitation interactions.

Deleted: metropolitan

Deleted: inhomogeneity of the spatial distribution of

Deleted: or loading

Deleted:

Deleted: inhomogeneity

Deleted: the spatial distribution of

Deleted: inhomogeneity

1. Introduction

It has been reported that there has been an increase in the frequency of torrential rain in urban areas over the last decades (Bouvette et al., 1982; Diem and Brown, 2003; Fujibe, 2003; Takahashi, 2003; Burian and Shepherd, 2005; Shepherd, 2005; Chen et al., 2015). Over the last decades, population in urban areas has increased significantly. In 1950, 30 % of the whole population in the world lived in urban areas, however, in 2010, 54 % of the whole population lived in urban areas. It is predicted that in 2050, 66 % of the whole population will live in urban areas (United Nations, 2015). In addition, urban areas are the centers of economic activity and play a key role in economic productivity (United Nations, 2015). Hence, the increase in the frequency of torrential rain, which has substantial negative impacts on human life and properties by causing events such as flooding and landslide, particularly in urban areas has important social and economic implications.

Torrential rain in urban areas frequently involves highly inhomogeneous spatial distributions of precipitation (Dhar and Nandergi, 1993; Mannan et al., 2013). While some places in a metropolitan area experience light precipitation, others in the area experience extremely heavy precipitation or torrential rain for an identical mesoscale convective system (MCS) that covers the whole area (e.g., Sauer et al., 1984; Korea Meteorological Administration, 2011). Note that this type of the MCS is forced by synoptic-scale temperature and humidity forcings. These "synoptic-scale" forcings tend to be spatially homogeneous in the MCS whose spatial scale is at mesoscale and thus much smaller than that of the forcings. Hence, these forcings tend to intensify all of cloud cells in the MCS in an approximately homogeneous fashion, which tend to produce cloud cells with a similar intensity. These cloud cells with the similar intensity are likely to result in a homogeneous distribution of precipitation over a domain of interest, since cloud cells with the similar intensity are likely to produce similar precipitation. This indicates that the consideration of the synoptic-scale forcings alone is not able to explain the occurrence of torrential rain which is associated with inhomogeneous spatial distributions of precipitation. Note that numerous numerical weather prediction studies have utilized the concept of the synoptic-scale forcings to identify mechanisms that

Deleted: or occurrence

Deleted: he t

Deleted: the

Deleted: districts

Deleted: city

Deleted: districts

Deleted: city

Deleted: city

Deleted: or large-scale

Deleted: the

Deleted: the

Deleted: the

control the inhomogeneity of precipitation distributions and associated torrential rain. This is one of the reasons these studies have shown low forecast accuracy for torrential rain and not been able to provide a clear picture of the mechanisms (Mladek et al., 2000; Yeh and Chen, 2004; Mannan et al., 2013). The highly inhomogeneous distribution of precipitation means that there are highly inhomogeneous variables, processes and forcings which disrupt the synoptic-forcing-induced homogeneity of MCSs in urban areas. Some of those forcings are mesoscale forcings that show mesoscale variability and, for example, are related to phenomena such as sea-breeze fronts and lake breezes. In particular, in urban areas, due to strong heat fluxes at the surface, there is the urban heat island (UHI) effect as another example of those phenomena. Examples of those variables and processes are cold pool, rear inflow, wind shear, and mesoscale vorticity. Aerosol is also one of those variables which have large spatial variability. In particular, urban aerosol particles are produced by randomly distributed sources (e.g., traffic), which enables aerosol to have large variability in urban areas.

It is well-known that increasing aerosol loading alters cloud microphysical properties such as cloud-particle size and autoconversion. Cloud-liquid particles, which are droplets, collide and collect each other to grow to be raindrops and this growth process is referred to as autoconversion. Collision and collection are more efficient when particle sizes are larger. Hence, increasing aerosol loading, which is known to reduce the particle size, reduces the efficiency of the growth of cloud-liquid particles to raindrops via autoconversion. This results in more cloud liquid which is not grown to be converted to raindrops and thus in more cloud-liquid mass as a source of evaporation and freezing. It has been shown that aerosol-induced increases in cloud-liquid mass and associated increases in freezing of cloud liquid can enhance parcel buoyancy and thus invigorate convection (Khain et al., 2005; Rosenfeld et al., 2008; Li et al., 2011; Wang et al., 2014). Invigorated convection can enhance precipitation. Studies (e.g., van den Heever et al., 2006; Fan et al., 2009; Lebo and Seinfeld, 2011; Lebo, 2017) have shown that aerosol-induced invigoration of convection and enhancement of precipitation depend on competition between aerosol-induced increases in buoyancy and those in hydrometeor loading, and aerosol-induced increases in condensational heating and associated invigoration in the warm sector of a cloud system. Other studies (e.g., Khain et al., 2008;

Deleted: the
Deleted: the
Deleted: or metropolitan
Deleted: e
Deleted: most representative
Deleted: that
Deleted: the
Deleted: high-degree
Deleted: inhomogeneity
Deleted: or moving
Deleted: the
Deleted: high-degree
Deleted: inhomogeneity
Deleted: .
Deleted: Droplets or
Deleted: c
Deleted: These c
Deleted: or
Deleted:
Deleted: .
Deleted: The i
Deleted: .
Deleted:

Lee et al., 2008b; Fan et al., 2009) have shown that the invigoration-related enhancement of precipitation also depends on environmental conditions that are represented by wind shear, relative humidity, and instability.

Aerosol-induced increases in cloud-liquid mass and associated increases in evaporation can intensify gust fronts, which in turn intensify subsequently developing convective clouds and enhance precipitation (Khain et al., 2005; Seifert and Beheng, 2006; Tao et al., 2007; van den Heever and Cotton, 2007; Storer et al., 2010; Tao et al., 2012; Lee and Feingold, 2013; Lee et al., 2017). Aerosol-induced invigoration and intensification of convection and associated convective clouds raise a hypothesis that the large spatial variability of aerosol in tandem with increasing aerosol loading can generate and enhance torrential rain which can involve the inhomogeneity of precipitation and associated cloud intensity in urban areas. For example, cloud cells (in an MCS) sitting on a significant portion of a metropolitan area with a higher aerosol concentration can be invigorated more than those cells on the rest portion of the area with a lower aerosol concentration. This can lead to enhanced precipitation and possibly torrential rain at the portion with the higher aerosol concentration, while in the rest portion, there can be less precipitation. This creates an inhomogeneity of precipitation distributions that can accompany torrential rain in the specific portion of the area. A further increase in aerosol concentration in the portion with the higher aerosol concentration will further enhance precipitation and torrential rain there and thus create a greater inhomogeneity of precipitation distributions. Motivated by the hypothesis and associated argument here, among the forcings, processes and variables which have spatial variability, this study focuses on aerosol. To examine aerosol effects on clouds and precipitation, numerical simulations are performed by using a cloud-system resolving model (CSRM) that resolves cloud-scale microphysical and dynamic processes and simulates the effect of the variability and loading of aerosol on precipitation.

Using the CSRM, an observed MCS that involves deep convective clouds and torrential rain is simulated. Here, deep convective clouds reach the tropopause. For the simulations, we select an MCS over the Seoul area (in Korea) that has a population of ~ twenty five millions and thus is one of representative conurbation areas around the world. These simulations are to identify key mechanisms that are associated with cloud-scale

Deleted: The a
Deleted: These a
Deleted: or
Deleted:
Deleted: the possibility
Deleted: high-degree inhomogeneity
Deleted: the
Deleted: district
Deleted: in a city
Deleted: other
Deleted: districts
Deleted: in the city
Deleted: district
Deleted: other districts
Deleted: the
Deleted: a
Deleted: area
Deleted: The
Deleted: loading
Deleted: at
Deleted: district
Deleted: the
Deleted: is
Deleted: n
Deleted: inhomogeneity
Deleted: the
Deleted: ten
Deleted: the
Deleted: metropolitan

microphysics and dynamics and explain the generation of the inhomogeneity of precipitation and associated torrential rain in terms of the spatial variability and loading of aerosol.

2. Case description

The MCS was observed in the Seoul area, Korea over a period between 09:00 LST (local solar time) July 27th and 09:00 LST July 28th 2011. A significant amount of precipitation is recorded during this period, with a local maximum value of ~ 200.0 mm hr^{-1}. This heavy rainfall caused flash floods and landslides, leading to the deaths of 60 people (Korea Meteorological Administration, 2011). At 21:00 LST July 26th 2011, favorable synoptic-scale features for the development of the selected MCS and heavy rainfall were observed. The western Pacific subtropical high (WPSH) was located over the southeast of Korea and Japan, and there was a low-pressure trough over north China (Figure 1). Low-level jets between the flank of the WPSH and the low-pressure system brought warm, moist air from the Yellow Sea to the Korean Peninsula (Figure 1). Transport of warm and moist air by the southwesterly low-level jet is an important condition for the development of heavy rainfall events over the Korean Peninsula (Hwang and Lee 1993; Lee et al. 1998; Sun and Lee 2002).

3. CSRM and simulations

3.1 CSRM

As a CSRM, we use the Advanced Research Weather Research and Forecasting (ARW) model (version 3.3.1), which is a nonhydrostatic compressible model. Prognostic microphysical variables are transported with a 5th-order monotonic advection scheme (Wang et al., 2009). Shortwave and longwave radiation parameterizations have been included in all simulations by adopting the Rapid Radiation Transfer Model (RRTMG; Mlawer et al., 1997; Fouquart and Bonnel, 1980). The effective sizes of hydrometeors are

Deleted: inhomogeneity

Formatted: Font: Bold

Formatted: Numbered + Level: 1 + Numbering Style: 1, 2, 3, … + Start at: 3 + Alignment: Left + Aligned at: 0.5" + Indent at: 0.75"

Formatted: Font: Bold

Formatted: List Paragraph, Outline numbered + Level: 2 + Numbering Style: 1, 2, 3, … + Start at: 1 + Alignment: Left + Aligned at: 1" + Indent at: 1.25"

Formatted: List Paragraph, Indent: Left: 0.75"

calculated in a microphysics scheme that is adopted by this study and the calculated sizes are transferred to the RRTMG. Then, the effects of the effective sizes of hydrometeors on radiation are calculated in the RRTMG.

To represent microphysical processes, the CSRM adopts a bin scheme. The bin scheme adopted is based on the Hebrew University Cloud Model (HUCM) described by Khain et al. (2011). The bin scheme solves a system of kinetic equations for size distribution functions for water drops, ice crystals (plate, columnar and branch types), snow aggregates, graupel and hail, as well as cloud condensation nuclei (CCN). Each size distribution is represented by 33 mass doubling bins, i.e., the mass of a particle m_k in the k bin is determined as $m_k = 2m_{k-1}$.

3.2 Control run

For a three-dimensional simulation of the observed MCS, i.e., the control run, two-way interactive triple-nested domains with a Lambert conformal map projection as shown in Figure 2 is adopted. A domain with a 500-m resolution covering the Seoul area (Domain 3) is nested in a domain with a 1.5-km resolution (Domain 2), which in turn is nested in a domain with a 4.5-km resolution (Domain 1). The length of Domain 3 in the east-west direction is 220 km, while the length in the north-south direction is 180 km. The lengths of Domain 2 and Domain 3 in the east-west direction are 390 and 990 km, respectively, and those in the north-south direction are 350 and 1100 km, respectively. The Seoul area is a conurbation area that centers in Seoul and includes Seoul and surrounding highly populated cities. Hence, the Seoul area is composed of multiple cities whose total population is ~twenty five millions. The boundary of Seoul, which has the largest population among those cities, is marked by a dotted line in Figure 2. Black contours in Figure 2 represent terrain heights. They indicate that most of high terrain is located on the eastern part of the Korean Peninsula and the Seoul area is not affected by high terrain. All domains have 84 vertical layers with a terrain following sigma coordinate, and the model top is 50 hPa. Note that a cumulus parameterization scheme is used in Domain 1 but not used in Domain 2 and Domain 3 where convective rainfall generation is assumed to be explicitly resolved. Here, we use a cumulus parameterization scheme that was developed

Deleted: the
Deleted: the
Deleted: by the CSRM
Deleted: 09
Deleted: the
Formatted: Font: Bold
Formatted: Font: Bold
Formatted: Font: Bold
Moved (insertion) [1]
Deleted: A
Deleted: is performed over a one-day period. The control run consists of
Deleted: (
Deleted: 1
Deleted:).
Deleted:
Deleted: the

by Kain and Fritsch (1990 and 1993). This scheme is shown to work reasonably well for resolutions that are similar to what is used for Domain 1 (Gilliland and Rowe, 2007).

Deleted:

Reanalysis data, which are produced by the Met Office Unified Model (Brown et al., 2012) and recorded continuously every 6 hours on a 0.11° × 0.11° grid, provide the initial and boundary conditions of potential temperature, specific humidity, and wind for the simulation. These data represent the synoptic-scale environment. For the control run, we adopt an open lateral boundary condition. Using the Noah land surface model (LSM; Chen and Dudhia, 2001), surface heat fluxes are predicted.

The current version of the ARW model assumes horizontally homogeneous aerosol properties. For the control run that focuses on the effect of aerosol on torrential rain in an urban area (i.e., Seoul area) where aerosol properties such as composition and number concentration vary significantly in terms of time and space, we abandon this assumption of homogeneity and consider the spatiotemporal variability of aerosol properties over the urban area. For this, we develop an aerosol module that is able to represent the variability of aerosol properties. This aerosol module interpolates observed background aerosol properties such as aerosol mass (e.g., PM_{10}) at observation sites to model grid points and time steps. This aerosol module is now implemented to the ARW model.

The variability of aerosol properties is observed by surface sites that measure PM_{10} in the Seoul area. These sites are distributed with about 1 km distance between them and measure aerosol mass every ~10 minutes, which enables us to resolve the variability with high spatiotemporal resolutions. However, the measurement of other aerosol properties such as aerosol composition and size distributions at those sites is absent. There are additional sites of the aerosol robotic network (AERONET; Holben et al., 2001) in the Seoul area. Distances between these AERONET sites are ~10 km, hence, they do not provide data whose resolutions are as high as those of the PM_{10} data. However, the AERONET sites provide information on aerosol composition and size distributions. While using data from the high-resolution PM_{10} sites to represent the variability of aerosol properties over the Seoul area, we use the relatively low-resolution data from the AERONET sites to represent aerosol composition and size distributions.

AERONET measurements indicate that overall, aerosol particles in the Seoul area during the MCS period follow a tri-modal log-normal distribution and aerosol particles,

on average, are an internal mixture of 60 % ammonium sulfate and 40 % organic compound. This organic compound is assumed to be water soluble and composed of (by mass) 18 % levoglucosan ($C_6H_{10}O_5$, density = 1600 kg m^{-3}, van't Hoff factor = 1), 41 % succinic acid ($C_6O_4H_6$, density = 1572 kg m^{-3}, van't Hoff factor = 3), and 41 % fulvic acid ($C_{33}H_{32}O_{19}$, density = 1500 kg m^{-3}, van't Hoff factor = 5) based on a simplification of observed chemical composition. This mixture is adopted to represent aerosol chemical composition in this study. Since the mixture includes chemical components that absorb solar radiation insignificantly as compared to strong radiation absorbers such as black carbon, we assume that the mixture does not absorb solar radiation and thus do not simulate the solar absorption of aerosol and attendant effects on stability. Based on the AERONET observation, in this study, the tri-modal log-normal distribution is assumed for the size distribution of background aerosol as exemplified in Figure 3. Stated differently, it is assumed that the size distribution of background aerosol at all grid points and time steps has size distribution parameters or the shape of distribution that is identical to that in Figure 3. The assumed shape of the size distribution of background aerosol is obtained by averaging size distribution parameters (i.e., modal radius and standard deviation of each of nuclei, accumulation and coarse modes, and the partition of aerosol number among those modes) over the AERONET sites and the MCS period. With these assumption and adoption, PM_{10} is converted to background aerosol number concentrations. Figures 4a and 4b show example spatial distributions of background aerosol number concentrations at the surface in Domain 3 (which covers the Seoul area), which are applied to the control run and represented by black contours. These distributions in Figures 4a and 4b are calculated based on the surface observation in Domain 3. Blue contours in Figures 4a and 4b surround areas with observed heavy precipitation on which this study focuses. In this study, when a precipitation rate at the surface is 60 mm hr^{-1} or above, precipitation is considered heavy precipitation. There is no one universal designated rate (of precipitation) above which precipitation is considered heavy precipitation and the designated rate varies among countries. 60 mm hr^{-1} as a precipitation rate is around the upper end of the variation. Those blue contours are further discussed below in Results. Purple lines in Figures 4a and 4b mark the eastern part of where there is substantial transition from high-value aerosol concentrations to

low-value aerosol concentrations. In this transition part, there is reduction in aerosol concentrations by more than a factor of 10 from ~9000 cm^{-3} to ~700 cm^{-3}.

In clouds, aerosol size distributions evolve with sinks and sources, which include advection and droplet nucleation (Fan et al., 2009). Aerosol activation is calculated according to the Köhler theory, i.e., aerosol particles with radii exceeding a critical value at a grid point are activated to become droplets based on predicted supersaturation, and the corresponding bins of the aerosol spectra are emptied. After activation, aerosol mass is transported within hydrometeors by collision-coalescence and removed from the atmosphere once hydrometeors that contain aerosols reach the surface. It is assumed that in the planetary boundary layer (PBL), background aerosol concentrations do not vary with height but above the PBL, background aerosol concentrations reduce exponentially with height. It is also assumed that in non-cloudy areas, aerosol size and spatial distributions are set to follow background counterparts. In other words, once clouds disappear completely at any grid points, aerosol size distributions and number concentrations at those points recover to background counterparts. This assumption has been used by numerous CSRM studies and proven to simulate overall aerosol properties and their impacts on clouds and precipitation reasonably well (Morrison and Grabowski, 2011; Lebo and Morrison, 2014; Lee et al., 2016). This assumption indicates that we do not consider the effects of clouds and associated convective and turbulent mixing on the properties of background aerosol. Also, above-explained prescription of those properties (e.g., number concentration, size distribution, and chemical composition) indicates that this study does not take aerosol physical and chemical processes into account. This enables the confident isolation of the sole effects of given background aerosol on clouds and precipitation in the Seoul area, which has not been understood well, by excluding those aerosol processes and cloud effects on background aerosol.

3.3 Additional runs

As seen in Figures 4a and 4b at 19:00 and 20:00 LST July 27th 2011, there is a large variability of background aerosol concentrations in the Seoul area. This variability is generated by contrast between the high aerosol concentrations in the western part of the

Formatted: Superscript

Formatted: Superscript

Deleted: ¶

Formatted: Font: Bold

Formatted: List Paragraph, Indent: Left: 0.75"

Moved up [1]: A three-dimensional simulation of MCS, i.e., the control run, is performed over a one-day period. The control run consists of two-way interactive triple-nested domains with a Lambert conformal map projection (Figure 1). A domain with a 500-m resolution covering the Seoul area (Domain 3) is nested in a domain with a 1.5-km resolution (Domain 2), which in turn is nested in a domain with a 4.5-km resolution (Domain 1). All domains have 84 vertical layers with a terrain following sigma coordinate, and the model top is 50 hPa. Note that the cumulus parameterization scheme is used in Domain 1 but not used in Domain 2 and Domain 3 where convective rainfall generation is assumed to be explicitly resolved. ¶

The MCS was observed over Seoul, Korea (09:00 LST (local solar time) July 27th – 09:00 LST July 28th 2011). A significant amount of precipitation is recorded during this period, with a local maximum value of ~ 200.0 mm hr^{-1}. This heavy rainfall caused flash floods and landslides, leading to the deaths of 60 people (Korea Meteorological Administration, 2011). At 21:00 LST July 26th 2011, favorable synoptic-scale features for the development of the selected MCS and heavy rainfall were observed. The western Pacific subtropical high (WPSH) was located over the southeast of Korea and Japan, and there was a low-pressure trough over north China (Figure 2). Low-level jets between the flank of the WPSH and the low-pressure system brought warm, moist air from the Yellow Sea to the Korean Peninsula (Figure 2). Transport of warm and moist air by the southwesterly low-level jet is an important condition for the development of heavy rainfall events over the Korean Peninsula (Hwang and Lee 1993; Lee et al. 1998; Sun and Lee 2002).¶

Reanalysis data, which are produced by the Met Office Unified Model (Brown et al., 2012) and recorded continuously every 6 hours on a 0.11° × 0.11° grid, provide the initial and boundary conditions of potential temperature, specific ...

Deleted: **3. Case description and simulations**¶ ¶ **3.1 Control run** ¶ ...

Deleted: ¶ ¶

Deleted: I

Deleted: 4

Deleted: 4

Formatted: English (U.S.)

Deleted: high-degree spatial inhomogeneity

Deleted: or Domain 3

Deleted: inhomogeneity

Deleted: the

domain where aerosol concentration is greater than 1500 cm^{-3}, and the low aerosol concentrations in the eastern part of the domain where aerosol concentration is ~700 cm^{-3} or less. As mentioned above, this study focuses on the effect of the spatial variability and loading (or concentrations) of aerosol on precipitation. To better identify and elucidate the effect, the control run is repeated but with above-mentioned contrast that is reduced. To reduce contrast, over the whole simulation period, the concentrations of background aerosol in the western part of the domain are reduced by a factor of 2, while those in the eastern part do not change. This means that the reduction in the variability accompanies that in aerosol concentrations, which enables us to examine both the effects of the variability and those of concentrations. Note that high and low aerosol concentrations on the left (or western) side and the right (or eastern) side of the domain, respectively, are maintained throughout the whole simulation period, although the location of the boundary between those sides changes with time. Here, in the process of the reduction in contrast, no changes are made for aerosol chemical compositions and size distributions in both parts of the domain. As examples, the spatial distribution of background aerosol concentrations at the surface with reduced contrast at 19:00 and 20:00 LST July 27th 2011 is shown in Figures 4c and 4d, respectively. With reduced contrast and concentrations, the variability and concentrations of aerosol are lower in this repeated run than in the control run. The repeated simulation has "low" variability and concentrations of "aerosol" as compared to the control run and thus is referred to as the low-aerosol run. Comparisons between the control run and the low-aerosol run give us a chance to better understand roles played by the spatial variability and loading of aerosol in the spatial distribution of precipitation which involves torrential rain.

In addition to the control run and the low-aerosol run, there are more simulations that are performed to better understand the effect of aerosol on precipitation here. To isolate the effects of aerosol concentrations on precipitation from those of aerosol spatial variability or vice versa, the control run and the low-aerosol run are repeated with homogeneous spatial distributions of aerosol. These homogeneous spatial distributions mean that there is no contrast in aerosol number concentrations between the western part of the domain and the eastern part, and aerosol number concentrations do not vary over the domain. The repeated simulations are referred to as the control-homoge run and the

Deleted: ¶
Deleted: inhomogeneity
Deleted: the
Deleted: or inhomogeneity
Deleted: the
Deleted: inhomogeneity
Deleted: inhomogeneity
Deleted: the
Deleted: the
Deleted: the
Deleted: the
Deleted: 4
Deleted: 4
Deleted: the
Deleted: or loading
Deleted: inhomogeneity
Deleted: the
Deleted: inhomogeneity
Deleted: the
Deleted: inhomogeneity

low-aerosol-homoge run. The analyses of model results below indicate that differences in precipitation between the control run and the low-aerosol run are closely linked to cloud-liquid evaporative cooling and to elucidate this linkage, the control run and the low-aerosol run are repeated again by turning off cooling from cloud-liquid evaporation. These repeated simulations are referred to as the control-noevp run and the low-aerosol-noevp run. While a detailed description of those repeated simulations is given in Section 4.3, a brief description is given in Table 1.

Deleted: the following sections

4. Results

In this study, analyses of results are performed only in the Seoul area (or Domain 3) where the 500-m resolution is applied. Hence, in the following, the description of the simulation results and their analyses are all only over Domain 3, unless otherwise stated.

4.1 Meteorological fields, microphysics and precipitation

Deleted: M

4.1.1 Meteorological fields and cumulative precipitation

Deleted: C

Formatted: Font: 12 pt

Deleted: ¶

Figure 5 shows the observed and simulated vertical profiles of potential temperature, water-vapor mass density, u-wind speed, and v-wind speed which represent meteorological fields. Radiosonde data as observation data are averaged over observation sites in the domain and the simulation period, while simulated meteorological fields are averaged over the domain and the simulation period to obtain the profiles. Positive (negative) u-wind speed represents eastward (westward) wind speed, while positive (negative) v-wind speed represents northward (southward) wind speed. Comparisons between the observed profiles and the simulated counterparts show that overall differences between them are within ~ 10% of observed values. Hence, with confidence, it can be considered that the simulation of meteorological fields is performed reasonably well.

The area-mean precipitation rate at the surface smoothed over 3 hours for the control run and the low-aerosol run is depicted by solid lines in Figure 6. Dotted lines in Figure 6 depict the precipitation rate for the repeated control run and low-aerosol run and will be discussed in Section 4.3. The simulated precipitation rate in the control run follows the observed counterpart well, which demonstrates that simulations perform reasonably well. Here, observed precipitation is obtained from measurement by rain gauges that are parts of the automatic weather system (AWS) at the surface. The AWS has a spatial resolution of ~3km. Also, the temporal evolution of the mean precipitation rate in the control run is very similar to that in the low-aerosol run. Associated with this similarity, the averaged cumulative precipitation over the domain at the last time step for the control run is 154.7 mm, which is just ~3 % greater than 150.2 mm for the low-aerosol run.

Deleted: 5

Deleted: are

Deleted: ed

Deleted: the

4.1.2 Precipitation fields and frequency distributions

Figures 7a, 7b and 7c show frequency distributions of precipitation rates that are collected over all of time steps and all of grid points at the surface in the simulations. In Figure 7, solid lines represent frequency distributions for the control run and the low-aerosol run, while dashed lines represent those for the repeated control run and low-aerosol run which will be described in Section 4.3. Figures 7a, 7d, 7g, 7j, and 7m show frequency distributions only for the control run and the low-aerosol run. The other panels in Figure 7 are supposed to show distributions only for the repeated control run and low aerosol run, however, for comparisons between the control run, the low-aerosol run, and the repeated runs, the control run and the low-aerosol run are displayed as well in those panels.

Deleted: 6

Deleted: s

Deleted: the

Deleted: simulations.

In Figures 7a, 7b, and 7c, frequency distributions of observed precipitation rates that are interpolated to grid points and time steps in the simulations are also shown. The observed maximum precipitation rate is ~180 mm hr^{-1}, which is similar to that in the control run. Also, observed frequency distribution is consistent well with the simulated counterpart in the control run, although it appears that particularly for heavy precipitation with rates above 60 mm hr^{-1}, the simulated frequency is underestimated as compared to the observed counterpart. The overall difference in frequency distributions between

Deleted: 6

Deleted: the

Deleted: those

Deleted: is

Deleted: the overall distribution of

Deleted: the

observation and the control run is much smaller than those between the control run and the low-aerosol run. Hence, we assume that the difference between observation and the control run is considered negligible as compared to that between the runs. Based on this, when it comes to a discussion about the difference between the control run and the low-aerosol run, results in the control run can be assumed to be benchmark results against which the effect of decreases in the spatial variability and concentrations of aerosol on results in the low-aerosol run can be assessed.

While we do not see a large difference in cumulative precipitation between the control run (154.7 mm) and the low-aerosol run (150.2 mm), the frequency distribution of precipitation rates shows distinctively different features between the control run and the low-aerosol run (Figure 7a). For precipitation with rates above 60 mm hr^{-1} or heavy precipitation, cumulative frequency is ~60 % higher for the control run. For certain ranges of precipitation rates above 60 mm hr^{-1}, there are increases in cumulative frequency by a factor of as much as ~10 to ~100. Moreover, for precipitation rates above 120 mm hr^{-1}, while there is the presence of precipitation in the control run, there is no precipitation in the low-aerosol run. Hence, we see that there are significant increases in the frequency of heavy precipitation in the control run as compared to that in the low-aerosol run.

Figure 8 shows spatial distributions of precipitation rates at the surface. Purple lines in Figure 8 mark the eastern part of where there is substantial transition from high-value aerosol concentrations to low-value aerosol concentrations as in Figure 4. In this transition part, as explained in Figure 4, there is reduction in aerosol concentrations by more than a factor of 10. Figures 8a and 8b show those distributions at 17:00 LST July 27th 2011 corresponding to initial stages of precipitating system in the control run and the low-aerosol run, respectively. At 17:00 LST, there is a small area of precipitation around the northwest corner of the domain in both the control run and the low-aerosol run. This implies that a small cloud system develops around the northwest corner of the domain at 17:00 LST. The size of the system and its precipitation area grow with time and at 19:00 LST, the size is much larger (Figures 8c and 8d). The maximum precipitation rate reaches ~100 mm hr^{-1} when time progresses to 19:00 LST (Figure 7d). Heavy precipitation is concentrated in a specific area (surrounded by the green rectangle) in both of the runs

Deleted: at

Deleted: the

Deleted: inhomogeneity

Deleted: two runs

Deleted: 6

Deleted: the

Deleted: the

Deleted: or occurrence

Deleted: or the occurrence

Deleted: or torrential rain

Deleted: 7

Deleted: the

Deleted: 7

Deleted: 7

Deleted: the

Deleted: In Figure 7, blue contours represent precipitation rates and the other contours are explained after the discussion of blue contours.

Deleted: 7

Deleted: 7

Deleted: 6

Deleted: b

(Figures 8c and 8d). The green rectangle surrounds a specific area where more than 90 % of the whole events of heavy precipitation (over the domain) with rates above 60 mm hr^{-1} occur in each of the runs at 19:00 LST. Since heavy precipitation starts to form around 19:00 LST, the green rectangle starts to be identified around 19:00 LST. Contrast in precipitation between the green rectangle and the other areas in the domain generates an inhomogeneity in the spatial distribution of precipitation. The location of the specific area in the control run is consistent well with the location of heavy precipitation in observation as seen in comparisons between Figures 4a, 8c, and 9a. Figure 9a shows the blue contour, which surrounds areas with observed heavy precipitation in Figure 4a, and the green rectangle, which surrounds the specific area where more than 90 % of the whole events of heavy precipitation occur in Figure 8c. In Figure 9a, the purple line, which marks the transition part where there is the substantial transition in aerosol concentrations in Figure 4a, is also shown. The good consistency between the locations demonstrates that the simulation of the spatial distribution of heavy precipitation is performed reasonably well. Between 17:00 LST and 19:00 LST, we do not see significant differences in the frequency distribution of precipitation rates, particularly in heavy precipitation with rates above 60 mm hr^{-1} between the control run and the low-aerosol run (Figure 7d).

By 20:00 LST, the maximum rate of torrential rain reaches ~130 mm hr^{-1} for the control run and ~110 mm hr^{-1} for the low-aerosol run (Figure 7g). Associated with this, between 19:00 and 20:00 LST, significant differences in frequency distributions, particularly for heavy precipitation between the control run and the low-aerosol run, start to appear (Figure 7g). At 20:00 LST as seen in Figure 8e and in the previous hours, in the control run, more than 90 % of heavy precipitation events are concentrated in a specific area that is surrounded by the green rectangle. Note that only in this specific area, extremely heavy precipitation with rates above 100 mm hr^{-1} occurs. In the low-aerosol run, the extremely heavy precipitation with rates above 100 mm hr^{-1} also occurs only in a particular area, which is surrounded by the green rectangle, at 20:00 LST (Figure 8f). At 20:00 LST, as seen in Figure 4b, observation shows that there are five spots of heavy precipitation. The location of the largest spot where most of heavy precipitation events occur is similar to that of the specific area that is surrounded by the green rectangle in the control run as seen in comparisons between Figures 4b, 8e and 9b. Figure 9b shows the

Deleted: 7
Deleted: 7
Deleted: at a specific time
Deleted:
Deleted: 4
Deleted: 7
Deleted: 8
Deleted: 8
Deleted: the
Deleted: 4
Deleted:
Deleted: 7
Deleted: for better observation of the consistency
Deleted:
Deleted: This
Deleted: runs
Deleted: 6
Deleted: b
Deleted: With the time progress to
Deleted: the maximum precipitation rate or
Deleted: 6c
Deleted: the
Deleted: runs
Deleted: 6c
Deleted: 7
Deleted: the
Deleted: the
Deleted: 7
Deleted: 4
Deleted: the
Deleted: the
Deleted: 4
Deleted: 7
Deleted: 8
Deleted: 8
Deleted: the

blue contour and the purple line in Figure 4b and the green rectangle in Figure 8e. This again demonstrates that the simulation of the spatial distribution of heavy precipitation is performed with fairly good confidence.

The system propagates eastwards after 20:00 LST in a way that its easternmost part is closer to the east boundary of the domain as seen in comparisons between Figure 8e (Figure 8f) and Figure 8g (Figure 8h) for the control (low-aerosol) run. As seen in Figure 8g and in the previous hours, for the control run, more than 90 % of heavy precipitation events are concentrated in a specific area (surrounded by the green rectangle) at 23:00 LST. However, in the low-aerosol run, heavy precipitation is not concentrated in a specific area at 23:00 LST. Unlike the green rectangle in the control run at 23:00 LST, the green rectangle at 23:00 LST in the low-aerosol run surrounds an area where ~50 % of heavy precipitation events are located, although the rectangle surrounds the largest area with heavy precipitation among heavy precipitation areas in the low-aerosol run. For a period between 20:00 and 23:00 LST as compared to that between 19:00 and 20:00 LST, the maximum precipitation rate rises up to ~180 mm hr^{-1} in the control run, however, in the low-aerosol run, the maximum precipitation rate stays at ~120 mm hr^{-1} (Figures 7g and 7j). Hence, there is the presence of precipitation rates between ~120 and ~180 mm hr^{-1} in the control run, while there is their absence in the low-aerosol run for the period between 20:00 and 23:00 LST. This reflects that increases in the frequency of torrential rain, which are induced by increases in the spatial variability and loading of aerosol, enhance, as the system evolves from its initial stage before 20:00 LST to mature stage between 20:00 and 23:00 LST.

Of interest is that the green rectangle is included in an area which is surrounded by the purple line in all panels with different times in Figure 8 and further discussion for this matter is provided in Section 4.2. After 23:00 LST July 27th 2011, the precipitating system enters its decaying stage. Figure 7m shows precipitation-rate frequency in the control run and the low-aerosol run for a period between 04:00 and 05:00 LST July 28th 2011. As seen in Figure 7m, with the progress of the decaying stage, the maximum precipitation rate reduces down to ~25 mm hr^{-1} as an indication that heavy precipitation disappears and the system is nearly at the end of its life cycle.

Deleted: 4
Deleted: and
Deleted: 7
Deleted: for better observation of the similarity
Deleted: continues to evolve
Deleted: 7
Deleted: 7
Deleted: 7
Deleted: 7
Deleted: the
Deleted: it appears that
Deleted: the
Deleted: the
Deleted: 6c
Deleted: 6d
Deleted: the
Deleted: inhomogeneity
Deleted: ¶
Deleted: 6e
Deleted: the
Deleted: 6e
Deleted: its
Deleted: the
Deleted:

4.2 Dynamics

4.2.1 Convergence

For the examination of condensation which is the main source of precipitation, convergence fields at the surface, where updrafts that produce condensation are originated, are obtained and the column-averaged condensation rates are superimposed on them. Other processes such as deposition and freezing produce the mass of solid hydrometeors and act as sources of precipitation, however, their contribution to precipitation is ~one order of magnitude smaller than that by condensation in the control run and the low-aerosol run. Hence, here, we zero in on condensation. Convergence and condensation fields are again superimposed on shaded precipitation fields as shown in Figure 10. In Figure 10, convergence and condensation fields are represented by white and yellow contours, respectively. When it comes to the convergence field in the green rectangle in Figure 10, which starts to be formed around 19:00 LST and is composed of convergence lines, the field in the rectangle in the control run is stronger than that in the low-aerosol run. The averaged intensity of the convergence field over an area with non-zero convergence in the green rectangle and over the simulation period is 0.013 s^{-1} in the control run, while the averaged intensity is 0.007 s^{-1} in the low-aerosol run. The convergence field in the green rectangle is strongest among convergence lines over the whole domain and, associated with this, stronger updrafts and greater condensation develop over that field in the green rectangle than in the other lines over the whole domain in each of the runs.

Figure 11 shows horizontal distributions of wind-vector field (arrows) superimposed upon fields of convergence, condensation, and precipitation. In general, particularly from 19:00 LST on, in the area with high-value aerosol concentrations to the west of the strong convergence field (surrounded by the green rectangle), there are greater horizontal wind speeds than in the area with low-value aerosol concentrations to the east of the strong convergence field in the control run. As seen in comparisons between the location of the rectangle and that of the purple line, which mark the transition zone for aerosol concentrations, the area to the west of the rectangle has higher aerosol concentrations

Deleted: As shown in Lee et al. (2008a and 2008b) and Khain et al. (2008), condensation acts as a main source of precipitation by providing cloud liquid as a source of accretion of cloud liquid by precipitable hydrometeors. Condensation is produced by updrafts that control supersaturation and updrafts are rooted in convergence around the surface. As the basic principle of dynamics indicates, air that converges around the surface induces upward motion (or updrafts) to satisfy mass conservation. The stronger convergence of air induces stronger updrafts and then more condensation. As a first step to the

Deleted:

Deleted: ation of

Deleted: at the surface

Deleted:

Deleted: and the

Deleted: superimposed

Deleted: as shown in Figure 7

Deleted:

Deleted: 7

Deleted: the

Deleted: red

Deleted: black

Deleted: The precipitation fields, which are represented by blue contours and discussed above, are displayed together with convergence and condensation fields in Figure 7.

Formatted: Superscript

Deleted: In Figures 7a and 7b, these fields at 17:00 LST around the initial stage of cloud development are shown in the control run and the low-aerosol run, respectively. Around the northwest corner of the domain, there is the initial formation of the convergence field in both the runs at 17:00 LST. The condensation and precipitation rates are on and around the convergence field in both the runs in Figures 7a and 7b due to above-mentioned fact that the convergence field induces updrafts which produce condensation and thus precipitation.¶ ...

Deleted: 9a

Deleted: the

Deleted: the

Deleted: at 19:00 LST in the control run

Deleted: the

Deleted: the

Deleted:

Deleted: is

Deleted: the stronger

Deleted: movement of air

Deleted: the

Deleted: the

than that to the east. In that area with high-value aerosol concentrations, there is greater cloud-liquid evaporation occurring than in that area with low-value aerosol concentrations in the control run as shown in Figure 12a. Figure 12a shows the vertical distribution of the time- and domain-averaged cloud-liquid and rain evaporation rates over each of the areas to the west and east of the strong convergence field, which is surrounded by the green rectangle, and over the period between 17:00 and 19:00 LST for the control run and the low-aerosol run. For the calculation of the averaged values in Figure 12, the area to the west (east) of the strong convergence field is set to include all parts of the north-south direction, which is the y-direction, and the vertical domains but a portion of the east-west direction domain, which is the x-direction domain that extends from the western boundary of Domain 3 to 90 km where the western boundary of the green rectangle at 19:00 LST is located (from 110 km where the eastern boundary of the green rectangle at 19:00 LST is located to the eastern boundary of Domain 3) in Domain 3 for the control run. For the low-aerosol run, the area to the west (east) of the strong convergence field is identical to that in the control run except for the fact that the area includes a portion of the x-direction domain that extends from the western boundary of Domain 3 to 70 km where the western boundary of the green rectangle at 19:00 LST is located (from 90 km where the eastern boundary of the green rectangle at 19:00 LST is located to the eastern boundary of Domain 3) in Domain 3.

High-value aerosol concentrations reduce autoconversion and in turn, increase cloud liquid as a source of evaporation and thus, increase cloud-liquid evaporation as compared to low-value aerosol concentrations. Also, with high-value aerosol concentrations, there is an increase in the surface-to-volume ratio of cloud droplets and this increases evaporation efficiency and thus, cloud-liquid evaporation as compared to the situation with low-value aerosol concentrations. However, mainly due to an increase in the size of raindrops and their associated decrease in the surface-to-volume ratio, which are induced by high-value aerosol concentrations, rain evaporation reduces as compared to the situation with low-value aerosol concentrations as also shown in van den Heever et al. (2011). Increases in cloud-liquid evaporation in turn enhance negative buoyancy, which induces stronger downdrafts in the area with high-value aerosol concentrations than in the area with low-value aerosol concentrations in the control run

Deleted: the
Deleted: the
Deleted: 0
Deleted: 0
Deleted:
Deleted: s
Comment [S1]: make figure for this
Deleted:
Deleted: (
Deleted:)
Deleted: 0
Deleted: (east)
Deleted: or
Deleted: or
Deleted: that
Deleted: 85 km where
Deleted: m 115 km where
Deleted: is located
Comment [S2]: should revise it later on.
Deleted:
Deleted: The h
Deleted: s
Deleted: s
Deleted:
Deleted: the
Deleted: the
Deleted: the
Deleted: the
Deleted: the
Deleted: the

particularly between 17:00 LST and 19:00 LST as seen in Figure 12b. Sublimation and melting also enhance negative buoyancy, however, their contribution is ~one order of magnitude smaller than the contribution by cloud-liquid evaporation. Hence, here, we focus on cloud-liquid evaporation. Figure 12b shows the vertical distribution of the time- and domain-averaged downdraft mass fluxes over each of the areas to the west and east of the strong convergence field (surrounded by the green rectangle) for the control run and the low-aerosol run over the period between 17:00 and 19:00 LST. Previous studies have shown that aerosol-induced increases in cloud-liquid evaporation are closely linked to the enhancement of the intensity of downdrafts (Lee et al., 2008a, b; Lee et al., 2013; Lee, 2017). Cloud liquid or droplets in downdrafts move together with downdrafts, thus, when downdrafts descend, cloud liquid descends while being included in downdrafts. Cloud liquid in the descending downdrafts evaporates. More evaporation of cloud liquid provides greater negative buoyancy to downdrafts so that they accelerate more (Byers and Braham, 1949; Grenci and Nese, 2001).

After reaching the near-surface altitudes below ~3 km, in the control run, stronger downdrafts spread out as stronger outflow or horizontal movement as seen in the area with high-value aerosol concentrations as compared to those in the area with low-value aerosol concentrations around 19:00 LST in Figure 11c. The outflow in the area with high-value aerosol concentrations accelerates, due to evaporation on its path, as it moves southeastwards from the northern and western boundaries of the domain. The outflow accelerates until it collides with surrounding air that has weaker horizontal movement in the area with low-value aerosol concentrations. This collision mainly occurs in the places where the transition between high-value aerosol concentrations and low-value aerosol concentrations is located (surrounded by the purple line) as seen in Figure 11c. This collision creates the strong convergence field around 19:00 LST, which is surrounded by the green rectangle in those places in the control run as seen in Figure 11c. Hence, most of the strong convergence field (surrounded by the green rectangle) is included in the transition zone between high-value and low-value aerosol concentrations (which is surrounded by the purple line) in the control run (Figure 11c). The strong convergence field in the green rectangle generates a large amount of condensation and cloud liquid and this large amount of cloud liquid produces not only heavy precipitation but also high-

Deleted: 0

Deleted: Figure 10b shows the vertical distribution of the time- and domain-averaged downdraft mass fluxes over each of the areas to the west and east of the strong convergence field (surrounded by the green rectangle) for the control run and the low-aerosol run over the period between 17:00 and 19:00 LST.

Deleted: 9

Deleted: a

Deleted: Then, stronger outflow in the area with high-value aerosol concentration

Deleted: or air with

Deleted: the

Deleted:

Deleted: or boundary

Deleted: the

Deleted: the

Deleted: red

Deleted: in Figure 4a

Deleted: s 4a and

Deleted: 9

Deleted: a

Deleted:

Deleted: s 7c and 9a

Comment [S3]: remove figure 8c in the old manuscript.

degree evaporation. Then, high-degree evaporation in turn contributes to the occurrence of a stronger convergence field in the green rectangle, which establishes feedbacks between the convergence field, condensation, heavy precipitation, and evaporation. This enables the intensification of downdrafts and horizontal wind to the west of the green-rectangle convergence field, the convergence field, and the increases in the heavy precipitation with time, while the green-rectangle convergence field is advected eastwards in the control run as seen in Figures 7g, 7j, 11e and 11g. As seen in Figures 11e and 11g, even after 19:00 LST, the green-rectangle convergence field stays within the transition zone between the high-value and low-value aerosol concentrations (which is surrounded by the purple line) during its eastward advection. This indicates that above-explained collision between strong outflow and surrounding weak wind, which is essential for the formation of the green-rectangle convergence field, continuously occurs in the transition zone even after 19:00 LST.

Note that, associated with aerosol concentrations in the western part of the domain, which are two times greater in the control run than in the low-aerosol run, there are two times greater differences in aerosol concentrations between the area with high-value aerosol concentrations and that with low-value aerosol concentrations in the control run than in the low-aerosol run. This leads to a two times greater transition in aerosol concentrations, particularly in the transition zone surrounded by the purple line in the control run than in the low-aerosol run (Figure 4). Associated with this, there are greater reduction in autoconversion and increases in cloud liquid and surface-to-volume ratio of cloud droplets in the area with high-value aerosol concentrations in the control run than in the low-aerosol run. Then, there are greater evaporation, intensity of downdrafts, associated outflow and its acceleration during its southeastward movement around the surface in that area in the control run than in the low-aerosol run (Figures 11 and 12). This means that there is stronger collision between outflow and the surrounding air in the control run than in the low-aerosol run, and stronger collision forms the strong convergence field (in the green rectangle) which is much more intense in the control run than in the low-aerosol run as seen in Figures 10 and 11. Over this much more intense convergence field, there is the formation of stronger updrafts that are able to form stronger convection, which is in turn able to produce more events of heavy precipitation

Deleted: the
Deleted:
Deleted: it
Deleted: moves
Deleted:
Deleted: is
Deleted: is
Deleted: the
Deleted: the
Deleted: reduction or
Deleted: area
Deleted: red
Deleted: 4
Deleted: the
Deleted: the
Deleted: and
Deleted: 9
Deleted: 0
Deleted: 7

in the control run than in the low-aerosol run (Figure 7). The more intense strong convergence field in the green rectangle establishes stronger feedbacks between the convergence field, condensation, heavy precipitation, and evaporation in the control run than in the low-aerosol run. Hence, differences in intensity of the green-rectangle convergence field and in the heavy precipitation between the runs get greater as time progresses (Figures 7, 10 and 11).

Deleted: 6
Deleted: the
Deleted: the
Deleted: s
Deleted: .

4.3 Sensitivity tests

4.3.1 Evaporative cooling

It is discussed that cloud-liquid evaporative cooling plays an important role in the formation of the strong convergence field where most of heavy precipitation occurs (surrounded by the green rectangle) in the control run. To confirm this role, we repeat the control run and the low-aerosol run with cooling from cloud-liquid evaporation turned off and cooling from rain evaporation left on. The repeated control run and the low-aerosol run are referred to as the control-noevp run and the low-aerosol-noevp run, respectively. In these repeated runs, cloud-liquid mass reduces due to cloud-liquid evaporation, although cloud-liquid evaporation does not affect temperature.

The temporal evolution of precipitation rates in the control-noevp run and the low-aerosol-noevp run is similar to that in the control run and the low-aerosol run (Figure 6a). However, due to the absence of cloud-liquid evaporative cooling, there is no formation of the strong outflow and convergence field (as seen in wind field and the green rectangle in the control run and the low-aerosol run) in these repeated runs as shown in Figures 13a and 13b. Figures 13a and 13b show wind-vector and convergence fields at the surface over the whole domain in the control-noevp run and the low-aerosol-noevp run, respectively, at 23:00 LST which corresponds to the mature stage of the system. Note that the strong convergence field is clearly distinguishable in its intensity and length from any other convergence lines in each of the control run and the low-aerosol run as seen in Figures 10 and 11. However, there is no field in each of the repeated runs that is distinguishable in their intensity and length from other lines as seen in Figures 13a and

Deleted: D
Deleted: 1
Deleted: 1
Deleted: 1
Deleted: 1
Deleted: the
Deleted: 7
Deleted: 1

13b. This leads to the situation where there is no particular convergence field in the control-noevp run that produces much more events of heavy precipitation than those in the low-aerosol-noevp run. As seen in Figures 7h and 7k, associated with this, differences in the frequency of heavy precipitation with rates above 60 mm hr^{-1} between the repeated runs are much smaller than those between the control run and the low-aerosol run particularly for the period between 19:00 LST and 23:00 LST, although the control-noevp run shows the greater frequency of heavy precipitation than the low-aerosol-noevp run. This results in much smaller differences in heavy precipitation between the repeated runs than between the control run and the low-aerosol run for the whole simulation period as seen in Figure 7b. This demonstrates that cloud-liquid evaporative cooling and its differences between the control run and the low-aerosol run play a key role in much more events of heavy precipitation in the control run than in the low-aerosol run.

4.3.2 Variability of aerosol concentrations

Remind that between the control run and the low-aerosol run, there are changes not only in the spatial variability of aerosol concentrations but also in aerosol concentrations. This means that differences between those runs are caused not only by changes in the variability but also by those in aerosol concentrations. Although there have been many studies on the effects of changes in aerosol concentrations on heavy precipitation, studies on those effects of changes in the variability have been rare. Motivated by this, as a preliminary step to the understanding of those effects of changes in the variability, here, we attempt to isolate the effects of changes in the variability on heavy precipitation from those in aerosol concentrations or vice versa. For this purpose, the control run and the low-aerosol run are repeated with homogeneous spatial distributions of background aerosol concentrations. These repeated runs are referred to as the control-homoge run and the low-aerosol-homoge run. In the control-homoge run (low-aerosol-homoge run), aerosol concentrations over the domain are fixed at one value, which is the domain-averaged concentration of the background aerosol in the control run (the low-aerosol run), at each time step. Hence, in the control-homoge run and the low-aerosol-homoge run, the variability (or contrast) in the spatial distribution of aerosol concentrations between the

Deleted: 1

Deleted: This in turn leads to the situation where

Deleted: is

Deleted: , on average, only ~10 % of

Deleted: This is seen in a comparison between the repeated runs, the control run, and the low-aerosol run in Figure 6f that shows the frequency for those runs over the period between 20:00 and 23:00 LST.

Deleted: comparison

Deleted: **Inhomogeneity**

Deleted: inhomogeneity in the spatial distribution

Deleted: e inhomogeneity

Deleted: or loading

Deleted: inhomogeneity

Deleted: homogeneity

Deleted: inhomogeneity

Deleted: he isolation

Deleted: al

Deleted: T

Deleted: has 2500 cm^{-3} as a concentration of the background aerosol over the whole domain and the whole simulation period. The low-aerosol-homoge run has 1400 cm^{-3} as a concentration of the background aerosol over the whole domain and the whole simulation period.

Deleted: inhomogeneity

Deleted: the

area with high-value aerosol concentrations and that with low-value aerosol concentrations is removed, which achieves homogeneous spatial distributions.

The temporal evolution of precipitation rates in the control-homoge run and the low-aerosol-homoge run is similar to that in the control run and the low-aerosol run (Figure 6b). However, with the homogeneity in the spatial distribution of aerosol concentrations, there is no formation of strong outflow and thus, strong convergence field that is distinguishable from any other convergence lines in the control-homoge run and low-aerosol-homoge run as seen in Figures 13c and 13d. Figures 13c and 13d show wind-vector and convergence fields over the whole domain at 23:00 LST in the control-homoge run and the low-aerosol-homoge run, respectively. In the absence of the variability between the area with high-value aerosol concentrations and that with low-value aerosol concentrations, there are no differences in evaporative cooling between those areas and thus, there are no strong outflow and thus, strong convergence field which is distinguishable from any other lines.

Comparisons between the control run and the control-homoge run (the low-aerosol run and the low-aerosol-homoge run) isolate the effects of the variability on heavy precipitation from those of aerosol concentrations whose averaged value is set at an identical value at each time step in the runs. Due to the absence of the variability in the spatial distribution of aerosol concentrations and the associated strong convergence field, the frequency of heavy precipitation in the control-homoge run and in the low-aerosol-homoge run is, on average, just ~18 and ~13 % of that in the control run and in the low-aerosol run, respectively, for the whole simulation period (Figure 7c). Hence, the presence of the variability alone (in the absence of changes in aerosol concentrations) increases the number of the heavy-precipitation events by a factor of ~ 5 or ~ 10. This presence alone also results in a substantial increase in the maximum precipitation rate in the control run and the low-aerosol run as compared to the repeated runs. Between the low-aerosol run and the low-aerosol-homoge run, the increase is from 80 mm hr^{-1} in the low-aerosol-homoge run to 120 mm hr^{-1} in the low-aerosol run, while between the control run and the control-homoge run, the increase is significant and from 90 mm hr^{-1} in the control-homoge run to 180 mm hr^{-1} in the control run (Figure 7c). Here, we see that even without the effects of changes in aerosol concentrations, the presence of the variability

Deleted: the
Deleted: the
Deleted: the
Deleted: The background aerosol concentration in the control-homoge run (the low-aerosol-homoge run) is the time- and domain-averaged concentration of the background aerosol in the control run (the low-aerosol run).
Deleted: W
Deleted: the
Deleted: 1
Deleted: 1
Deleted: 1
Deleted: 1
Deleted: the
Deleted: inhomogeneity
Deleted: the
Deleted: the
Deleted: and outflow
Deleted: is
Deleted: no
Deleted: inhomogeneity
Deleted: 2500
Deleted: (1400) cm^{-3}
Deleted: for both of
Deleted: inhomogeneity
Deleted: 2
Deleted: 0
Deleted: , over the mature stage
Deleted:
Deleted: 6g
Deleted: inhomogeneity
Deleted: over the mature stage
Deleted: 6g
Deleted: inhomogeneity

alone is able to cause the significant enhancement of heavy precipitation in terms of its frequency and maximum value.

Remember that there is an identical domain-averaged background aerosol concentration at each time step between the control run and the control-homoge run and between the low-aerosol run and the low-aerosol-homoge run. Hence, changes in the averaged aerosol concentration between the control-homoge run and the low-aerosol-homoge run are identical to those between the control run and the low-aerosol run. With these identical changes in the averaged aerosol concentration, between the control run and the low-aerosol run, there are additional changes in the variability of aerosol distributions. There is the larger frequency of heavy precipitation in the control-homoge run than in the low-aerosol-homoge run (Figure 7c). However, as mentioned above, there is no strong convergence field which is distinguishable from any other lines in the control-homoge run as seen in Figure 13c. Associated with this, differences in the frequency of heavy precipitation between the control-homoge run and the low-aerosol-homoge run are much smaller than those between the control run and the low-aerosol run particularly during the period between 19:00 LST and 23:00 LST, as seen in Figures 7i and 7l. This results in a situation where differences in the frequency of heavy precipitation between the control-homoge run and the low-aerosol-homoge run are, on average, just ~15 % of those between the control run and the low-aerosol run for the whole simulation period (Figure 7c). With identical changes in the averaged aerosol concentration between a pair of the control run and the low-aerosol run and a pair of the control-homoge run and the low-aerosol-homoge run, this demonstrates that additional changes in the variability of aerosol distributions play a much more important role in aerosol-induced increases in the occurrence of heavy precipitation than changes in the averaged aerosol concentrations.

5. Summary and conclusion

This study examines how aerosol affects heavy precipitation in an urban conurbation area. For this examination, a case that involves an MCS and torrential rain over the conurbation area which centers in Seoul, Korea is simulated. This case has large spatial

Deleted: the
Deleted: is
Deleted: hat
Deleted: is
Deleted: is an
Deleted: homogeneity
Deleted: The absence of
Deleted: the
Deleted: in the control-homoge run
Deleted: results in the situation where the increase in the frequency of heavy precipitation in the control-homoge run as compared to that in the low-aerosol-homoge run is,
Deleted: 10
Deleted: e increase
Deleted: in
Deleted: as compared to
Deleted: over the mature stage between 20:00 and 23:00 LST
Deleted: 6g
Deleted: the
Deleted: the
Deleted: inhomogeneity
Deleted: s
Deleted: the
Deleted: or torrential rain
Deleted: metropolitan
Deleted: the

variability in aerosol concentrations which involves high-value aerosol concentrations in the western part of the domain and low-value aerosol concentrations in the eastern part of the domain.

It is well-known that increases in aerosol concentrations reduce autoconversion and increase cloud liquid as a source of evaporation, which enhance evaporation and associated cooling. Hence, high-value aerosol concentrations in the western part of the domain cause high-value evaporative cooling rates, while low-value aerosol concentrations in the eastern part of the domain cause low-value evaporative cooling rates. Greater evaporative cooling produces greater negative buoyancy and more intense downdrafts in the western part than in the eastern part. More intense downdrafts then turn into stronger outflow over the western part that collides with surrounding air over the eastern part to form a strong convergence field along the boundary between those parts. Over this strong convergence field, most of heavy precipitation forms. When contrast in aerosol concentrations between the western and eastern parts, which represents the spatial variability in aerosol concentrations, reduces together with reducing aerosol concentrations over the western part, differences in evaporative cooling and outflow between those parts decrease substantially. This results in a much weaker convergence field along the boundary, which is followed by much less occurrences of heavy-precipitation events as compared to those with greater contrast. It is found that the changing variability has much more impacts on heavy precipitation than the changing aerosol loading.

Studies (e.g., Niyogi et al., 2006; Thielen et al., 2000) have shown that at the edge of a metropolitan area, due to stark contrast in the surface roughness (representing the surface property) between the area and surrounding rural areas, there are enhanced convergence and updrafts. The urban heat island (UHI) effect, which is associated with the surface property in metropolitan areas, also results in enhanced convergence and updrafts at the edge of the area (Ryu et al., 2013; Schmid and Niyogi, 2017). In addition, a metropolitan area has stronger and more aerosol sources than surrounding rural areas, hence, contrast in aerosol concentrations at the edge of a metropolitan area or at the urban/rural boundary, which is characterized by contrast in the surface property between the urban and rural areas, is unlikely to be rare. This study suggests that in case there is

Deleted: high-degree inhomogeneity of
Deleted: spatial distributions
Deleted:
Deleted: the
Deleted: the
Deleted: the
Deleted: s
Deleted: the
Deleted: s
Deleted: or torrential rain
Deleted: the
Deleted: or
Deleted: inhomogeneity
Deleted: of
Deleted: spatial distributions
Deleted: loading
Deleted: the
Deleted: s
Deleted: the
Deleted: inhomogeneity
Deleted: city
Deleted: a
Deleted: city
Deleted: the
Deleted: city
Deleted: city
Deleted: city
Deleted: the
Deleted: ci
Deleted: ty or
Deleted: the

this type of contrast in aerosol properties such as aerosol concentration at the boundary, there can be enhanced convergence and updrafts at the edge of a metropolitan area. Hence, this study suggests that urban/rural contrast in aerosol should be considered as an additional factor (in addition to contrast in the surface roughness and the UHI effect) to understand the enhancement of convergence and updrafts at the edge of a metropolitan area.

It should be noted that urban surface properties, which are represented by the roughness and control the UHI effect, and their contrast with the rural surface properties do not vary significantly with respect to time and space as compared to the variation of aerosol properties. Hence, the location of the urban/rural boundary does not change with time and space significantly. However, in contrast to this, aerosol properties vary substantially with respect to time and space and thus the location of boundary between high-aerosol concentrations and low-aerosol concentrations vary with respect to time and space substantially. For example, in a place such as a large-scale industrial complex within an urban area away from an urban boundary, there can be an increase in aerosol concentrations and thus high aerosol concentrations. These high aerosol concentrations can advect, as exemplified in the case adopted in this study, and a boundary between a place with low-aerosol concentrations and a place with high aerosol concentrations can vary spatiotemporally within the urban area. This indicates that the boundary between the place with high-aerosol concentrations and that with low-aerosol concentrations does not necessarily have to be co-located with the urban/rural boundary which is characterized by contrast in the surface property between urban and rural areas and whose location does not change much with respect to time and space. Demonstrating this, in this study, the high-aerosol/low-aerosol boundary, which is, for example, surrounded by the purple line in Figures 4a and 4b, is not co-located with the urban/rural boundary but located in the middle of the Seoul area. Considering that on the high-aerosol/low-aerosol boundary, heavy precipitation is concentrated in this study, a spatiotemporal variation of the boundary leads to a spatiotemporal variation of heavy precipitation within an urban area as shown in this study. Hence, while previous theories on urban heavy precipitation can explain heavy precipitation on urban/rural boundaries (characterized by the surface-property contrast) and are not able to explain heavy precipitation in various locations

Deleted: city
Deleted: the
Deleted: the
Deleted: city
Deleted: the
Deleted: city
Deleted: the
Deleted: city
Deleted: sudden
Deleted: in traffic and due to the movement of this traffic, the location of this increase can vary spatiotemporally
Deleted: Then,
Deleted: the
Deleted: the
Deleted: the sudden increase in traffic or high-aerosol concentrations
Deleted: city
Deleted: the
Deleted: the
Deleted: red
Deleted: 4
Deleted: 4
Deleted: domain or
Deleted: the
Deleted: or torrential rain
Deleted: city
Deleted: y

within an urban area, the findings in this study elucidate a mechanism behind heavy precipitation in various locations in an urban area and thus give us more comprehensive understanding of torrential rain in urban areas.

There are numerous factors that control the spatial distribution of updrafts and associated condensation. Note that changes in this distribution induce those in the spatial distribution of precipitation that may involve the generation and the enhancement of torrential rain. One of the factors is found to be increasing aerosol concentrations by previous studies (e.g., Khain et al., 2005; Seifert and Beheng, 2006; van den Heever and Contton, 2007; Tao et al., 2007; Storer et al., 2010; Tao et al., 2012; Lee and Feingold, 2013; Lee et al., 2017). These previous studies have found that increasing aerosol concentrations can alter the vertical and horizontal gradient of latent heating and cooling by altering the spatial distributions of freezing, evaporation, and condensation. This alteration leads to that in updrafts, cloud cells, and precipitation, which involves the generation and the enhancement of torrential rain. However, these studies have focused only on increasing aerosol concentrations and assumed that background aerosol concentrations are spatially distributed in a homogeneous fashion, hence, have not considered the effect of the spatial variability in aerosol on the spatial distribution of latent-heat processes, cloud dynamics, and precipitation. For example, the previous studies have found that aerosol-induced localized changes in evaporation for individual cloud cells can create subsequent localized changes in the horizontal gradient of latent cooling and temperature in and around individual cloud cells. Note that each of these individual localized changes is limited to each of individual localized areas in and around each of individual cloud cells. These changes lead to the generation and the enhancement of torrential rain in and around individual cloud cells. It is found that increasing spatial variability in aerosol concentrations also increases the gradient of evaporation and temperature. These changes lead to increases in the occurrence of heavy precipitation in a specific area which is along the high-aerosol/low-aerosol boundary and is not limited to a localized area in and around a cloud cell. It is demonstrated that increasing variability plays a much more important role in aerosol-induced increases in the occurrence of heavy precipitation than increases in aerosol concentrations with their homogeneous spatial distributions.

Deleted: city

Deleted: city

Deleted: of or

Deleted: s

Deleted: or

Deleted: or

Deleted: inhomogeneity of aerosol spatial distribution

Deleted: or

Deleted: the

Deleted: inhomogeneity

Deleted: of

Deleted: changes or

Deleted: the

Deleted: the

Deleted: inhomogeneity

Deleted: the

Deleted: ¶

Acknowledgements

This study is supported by the United States National Oceanic and Atmospheric Administration (Grant NOAA-NWS-NWSPO-2015-2004117), and the National Strategic Project-Fine particle of the National Research Foundation of Korea (NRF) funded by the Ministry of Science and ICT (MSIT), the Ministry of Environment (ME), and the Ministry of Health and Welfare (MOHW) (NRF-2017M3D8A1092022). This study is also supported by the GEMS program of the Ministry of Environment, Korea and the Eco Innovation Program of KEITI (2012000160003).

Deleted: ¶

References

Bouvette T, Lambert JL, and Bedient PB (1982) Revised rainfall frequency analysis for Houston. J Hydraul Div Proc Amer Soc Civil Eng 108: 515–528.

Brown A, Milton S, Cullen M, Golding B, Mitchell J, and Shelly A (2012) Unified modeling and prediction of weather and climate: A 25-year journey. Bull Am Meteorol Soc 93: 1865–1877.

Burian SJ, and Shepherd JM (2005) Effects of urbanization on the diurnal rainfall pattern in Houston: Hydrological processes. Rainfall Hydrol Proc 19: 1089–1103.

Byers HR, and Braham RR (1949) The thunderstorm U. S. Weather Bur., Washington, D. C.: 287 pp.

Chen F, and Dudhia J (2001) Coupling an advanced land-surface hydrology model with the Penn State-NCAR MM5 modeling system. Part I: Model description and implementation. Mon Wea Rev 129: 569–585.

Chen S., et al. (2015) Urbanization effect on precipitation over the Pearl River Delta based on CMORPH data. Adv Clim Chang Res 6: 16-22.

Dhar, ON, and Nandergi, S (1993) The zones of severe rainstorm activity over India. Int J Climatol13: 301-311.

Diem JE, and Brown DP (2003) Anthropogenic impacts on summer precipitation in central Arizona. USA Prof Geogr 55: 343–355.

Fan J,, Yuan, T., Comstock, , J. M., et al. (2009) Dominant role by vertical wind shear in regulating aerosol effects on deep convective clouds. J Geophys Res114: doi:10.1029/2009JD012352.

Fouquart Y, and Bonnel B (1980) Computation of solar heating of the Earth's atmosphere: a new parameterization. Beitr Phys Atmos 53: 35-62.

Fujibe F (2003) Long-term surface wind changes in the Tokyo metropolitan area in the afternoon of sunny days in the warm season. J Meteor Soc Japan 81: 141–149.

Gilliland EK, and Rowe CM (2007) A comparison of cumulus parameterization schemes in the WRF model. Proceedings of the 87th AMS annual meeting: available at https://ams.confex.com/ams/pdfpapers/120591.pdf

Grenci LM, and Nese JM (2001) A world of weather: fundamentals of meteorology: a

text/ laboratory manual, Kendall/Hunt Publishing Company.

Holben BN, Tanré D, Smirnov A, Eck TF, Slutsker I, Abuhassan N, Newcomb W W, Schafer JS, Chatenet B, Lavenu F, Kaufman YJ, Castle JV, Setzer A, Markham B, Clark D, Frouin R, Halthore R, Karneli A, O'Neill NT, Pietras C, Pinker RT, Voss K, and Zibordi G (2001) An emerging ground-based aerosol climatology: Aerosol optical depth from AERONET. J Geophys Res 106: 12067–12097.

Hwang S-O, and Lee D-K (1993) A study on the relationship between heavy rainfalls and associated low-level jets in the Korean peninsula. J Korean Meteorol Soc 29: 133–146.

Kain JS, and Fritsch JM (1990) A one dimensional entraining/detraining plume model and its application in convective parameterization. J Atmos Sci 47: 2784-2802.

Kain JS, and Fritsch JM (1993) Convective parameterization for mesoscale models: The Kain-Fritsch scheme. The representation of cumulus convection in numerical models. Meteor Monogr, No. 24, Amer Meteor Soc: 165-170.

Khain A, BenMoshe N, and Pokrovsky A (2008) Factors determining the impact of aerosols on surface precipitation from clouds: Attempt of classification. J Atmos Sci 65: 1721-1748.

Khain A, Pokrovsky A, Rosenfeld D, Blahak U, and Ryzhkoy A (2011), The role of CCN in precipitation and hail in a mid-latitude storm as seen in simulations using a spectral (bin) microphysics model in a 2D dynamic frame, Atmos Res, 99: 129–146.

Khain A, Rosenfeld D, and Pokrovsky A (2005) Aerosol impact on the dynamics and microphysics of deep convective clouds. Quart J Roy Meteor Soc 131: 2639-266..

Korea Meteorological Administration (2011) Heavy rainfall events top 10, KMA registered Pub., No. 11-136000-000833-01, Seoul, Korea, 48 p.

Lebo Z (2017) A numerical investigation of the potential effects of aerosol-induced warming and updraft width and slope on updraft intensity in deep convective clouds. J Atmos Sci: doi:10.1175/JAS-D-16-0368.1.

Lebo ZJ, and Morrison H (2014) Dynamical effects of aerosol perturbations on simulated idealized squall lines. Mon Wea Rev 142: 991-1009.

Lebo ZJ and Seinfeld JH (2011) Theoretical basis for convective invigoration due to

Deleted: .

Deleted: .

Deleted: .

Deleted: Khain A. (2009) Notes on state-of-the-art investigations of aerosol effects on precipitation: a critical review. Environ Res Lett 4: doi:10.1088/1748-9326/4/1/015004.¶

Formatted: Font: Not Italic

Formatted: Font: Not Bold

increased aerosol concentration. Atmos Chem Phys 11: 5407–5429.

Lee D-K, Kim H-R, and Hong S-Y (1998) Heavy rainfall over Korea during 1980–1990. Korean J Atmos Sci 1: 32–50.

Lee SS, Donner LJ, Phillips VTJ, and Ming Y (2008a) Examination of aerosol effects on precipitation in deep convective clouds during the 1997 ARM summer experiment. Q J R Meteorol Soc 134: 1201-1220.

Lee SS, Donner LJ, Phillips VTJ, and Ming Y (2008b) The dependence of aerosol effects on clouds and precipitation on cloud-system organization, shear and stability. J Geophys Res 113: D16202.

Lee SS, and Feingold G (2013) Aerosol effects on the cloud-field properties of tropical convective clouds. Atmos Chem Phys 13: 6713-6726.

Lee SS, Li Z, Mok J, et al. (2017) Interactions between aerosol absorption, thermodynamics, dynamics, and microphysics and their impacts on clouds and precipitation in a multiple-cloud system. Clim Dyn: https://doi.org/10.1007/s00382-017-3552-x, 2017.

Lee SS, Kim B-G, and Yum SS, et al. (2016) Effect of aerosol on evaporation, freezing and precipitation in a multiple cloud system. Clim Dyn 48: 1069-1087.

Li Z, Niu F, Fan J, Liu Y, Rosenfeld D, and Ding Y (2011) Long-term impacts of aerosols on the vertical development of clouds and precipitation. Nat Geosci 4: 888-894.

Mannan Md A, Chowdhury Md A, and Karmakar S (2013) Application of NWP model in prediction of heavy rainfall in Bangladesh, Pac. Sci. 56: 667-675.

Mladek, et al. (2000) Intercomparison and evaluation of precipitation forecasts for MAP seasons 1995 and 1996. Meteorol Atmos Phys 72: 111-129.

Mlawer EJ, Taubman SJ, Brown PD, Iacono MJ, and Clough SA (1997) RRTM, a validated correlated-k model for the longwave. J Geophys Res 102: 16663-1668.

Morrison H, and Grabowski WW (2011) Cloud-system resolving model simulations of aerosol indirect effects on tropical deep convection and its thermodynamic environment. Atmos Chem Phys 11: 10503–10523.

Niyogi D, Holt T, Zhong S, Pyle PC, and Basara J (2006) Urban and land surface effects on the 30 July 2003 mesoscale convective system event observed in the southern

Deleted: ¶

1804 Great Plains. J Geophys Res 111: 1–20.
1805 Rosenfeld D, Lohmann U, Raga GB, et al (2008) Flood or drought, How do aerosols
1806 affect precipitation? Science 321: 1309-1313.
1807 Ryu Y-H, Baik J-J, and Han J-Y (2013) Daytime urban breeze circulation and its
1808 interaction with convective cells. Q J R Meteorol Soc 139: 401–413.
1809 Sauer VB, Thomas WO, Stricker VA, and Wilson KV (1984) Flood characteristics of
1810 urban watersheds in the United States, United States Geological Survey Water-
1811 Supply Paper 2207, pp 63.
1812 Schmid PE, and Niyogi D (2017) Modeling urban precipitation modification by spatially
1813 heterogeneous aerosols. J Appl Meteorol Climatol: https://doi.org/10.1175/JAMC-
1814 D-16-0320.1.
1815 Seifert A, and Beheng KD (2006) A two-moment cloud microphysics parameterization
1816 for mixed-phase clouds. Part 2: Maritime vs. continental deep convective storms.
1817 Meteorol Atmos Phys 92: 67-82.
1818 Shepherd, JM (2005) A review of current investigations of urban-induced rainfall and
1819 recommendations for the future. Earth Interact 9: 1-27.
1820 Storer RL, van den Heever SC, and Stephens GL (2010) Modeling aerosol impacts on
1821 convection under differing storm environments. J Atmos Sci 67: 3904-3915. Sun J,
1822 and Lee T-Y (2002) A numerical study of an intense quasistationary convection band
1823 over the Korean peninsula. J Meteorol Soc Jpn 80: 1221–1245.
1824 Sun J,, and Lee T-Y (2002) A numerical study of an intense quasistationary convection
1825 band over the Korean peninsula. J Meteorol Soc Jpn 80:1221–1245.
1826 Takahashi H (2003) Secular variation in the occurrence property of summertime daily
1827 rainfall amount in and around the Tokyo metropolitan area (in Japanese with an
1828 English abstract). Tenki 50: 31–41.
1829 Tao W-K, Chen J-P, Li Z., Wang C, and Zhang C (2012) Impact of aerosols on convective
1830 clouds and precipitation. Rev Geophys 50: RG2001.
1831 Tao W-K, Li X, Khain A, Matsui T, Lang S, and Simpson J (2007) Role of atmospheric
1832 aerosol concentration on deep convective precipitation: Cloud-resolving model
1833 simulations. J Geophys Res 112: D24S18.
1834 Thielen J, Wobrock W, Gadian A, Mestayer P, and Creutin J-D (2000) The possible

influence of urban surfaces on rainfall development: a sensitivity study in 2D in the meso-γ-scale, Atmos Res 54: 15–39.

United Nations (2015) Department of Economic and Social Affairs, Population Division: World urbanization prospects: The 2014 Revision, (ST/ESA/SER.A/366), https://esa.un.org/unpd/wup.

van den Heever SC, Carrió GG, Cotton WR, DeMott PJ, and Prenni AJ (2006) Impacts of nucleating aerosol on florida storms. part I: Mesoscale simulations. J Atmos Sci 63: 1752–1775.

van den Heever SC., and Cotton WR (2007) Urban aerosol impacts on downwind convective storms. J Appl Meteorol Clim 46: 828–850.

van den Heever SC., Stephens GL., and Wood NB (2011) Aerosol indirect effects on tropical convection characteristics under conditions of radiative-convective equilibrium, J Atmos Sci 68: 699–718.

Wang H, Skamarock WC, and Feingold G (2009) Evaluation of scalar advection schemes in the Advanced Research WRF model using large-eddy simulations of aerosol-cloud interactions. Mon Wea Rev 137: 2547-2558.

Wang Y, Zhang R, Saravanan R (2014) Asian pollution climatically modulates mid-latitude cyclones following hierarchical modelling and observational analysis. Nature Comm 5: 3098.

Yeh H-C, and Chen GT-J (2004) Case study of an unusually heavy rain event over eastern Taiwan during the Mei-Yu Season. Mon Wea Rev 132: 320-337.

Deleted: ¶

FIGURE CAPTIONS

Figure 1. 850 hPa wind (m s^{-1}; arrows), geopotential height (m; contours), and equivalent potential temperature (K; shaded) at 21:00 LST July 26th 2011 over Northeast Asia. The rectangle in the Korean Peninsula in the panel marks Domain 3 that is explained in Section 3.2 and shown in Figure 2.

Figure 2. Triple-nested domains used in the CSRM simulations. The boundary of the figure itself is that of Domain 1, while the rectangles marked by "d02" and "d03" represent the boundary of Domain 2 and Domain 3, respectively. The dotted line represents the boundary of Seoul and terrain heights are contoured every 250 m.

Figure 3. Aerosol size distribution at the surface. N represents aerosol number concentration per unit volume of air and D represents aerosol diameter.

Figure 4. Spatial distributions of background aerosol number concentrations at the surface (black contours; in "× 10^3 cm^{-3}") and the boundary of each area that has precipitation rate of 60 mm hr^{-1} or above (blue contours) in Domain 3 at (a) 19:00 LST and (b) 20:00 LST. Purple lines in panels (a) and (b) mark a part of the domain where there is a substantial reduction in aerosol number concentrations (see text for the details of purple lines). Panels (c) and (d) are the same as panels (a) and (b), respectively, but with reduced contrast in aerosol number concentrations for the low-aerosol run (see text for the details of reduced contrast).

Figure 5. Vertical distributions of the averaged (a) potential temperature, (b) water vapor mass density, (c) u-wind speed, and (d) v-wind speed. Positive (negative) u-wind speed represents eastward (westward) wind speed, while positive (negative) v-wind speed represents northward (southward) wind speed. Observations are averaged over observation sites in Domain 3 and the simulation period, while simulations are averaged over Domain 3 and the simulation period.

Deleted: ¶
¶
¶
¶

Deleted: 1

Moved (insertion) [4]

Deleted: Figure 2. 850 hPa wind (m s^{-1}; arrows), geopotential height (m; contours), and equivalent potential temperature (K; shaded) at 21:00 LST July 26th 2011 over Northeast Asia. The rectangle in the Korean Peninsula in the panel marks Domain 3. ¶
¶
Figure 3. Aerosol size distribution at the surface. N represents the aerosol number concentration per unit volume of air and D represents the aerosol diameter.¶
¶

Moved up [4]: Figure 3. Aerosol size distribution represents the aerosol number concentration per unit volume of air and D represents the aerosol diameter.¶
¶

Deleted: 4

Deleted: Red

Deleted: red

Deleted: the

Deleted: the

Figure 6. Time series of the area-mean precipitation rates at the surface smoothed over 3 hours for the control run, the low-aerosol run, and observation in Domain 3. In panel (a), the rates in the control-noevp run and the low-aerosol-noevp are additionally shown, while in panel (b), the rates in the control-homoge run and the low-aerosol-homoge are additionally shown.

Figure 7. Frequency distributions of the precipitation rates at the surface, which are collected over the whole domain, for (a), (b), and (c) the whole simulation period, (d), (e), and (f) a period between 17:00 and 19:00 LST, (g), (h), and (i) a period between 19:00 and 20:00 LST, (j), (k), and (l) a period between 20:00 and 23:00 LST, and (m), (n), and (o) a period between 04:00 and 05:00 LST. In panels (a), (b), and (c) observed frequency which is interpolated to the simulation time steps and grid points is also shown.

Figure 8. Spatial distributions of precipitation rates at the surface. Green rectangles mark areas with heavy precipitation and are described in detail in text. Purple lines mark the eastern part of where there is substantial transition from high-value aerosol concentrations to low-value aerosol concentrations as in Figure 4. Panels (a), (c), (e) and (g) are for the control run, while panels (b), (d), (f) and (h) are for the low-aerosol run. Panels (a) and (b) are for 17:00 LST, and panels (c) and (d) are for 19:00 LST, while panels (e) and (f) are for 20:00 LST, and panels (g) and (h) are for 23:00 LST.

Figure 9. Boundary of each area which has the observed surface precipitation rate of 60 mm hr^{-1} or above (blue contours) and a specific area (surrounded by the green rectangle in the control run and described in text related to Figure 8) where heavy precipitation is concentrated in the control run in Domain 3 at (a) 19:00 LST and (b) 20:00 LST. Purple lines are the same as in Figure 8.

Figure 10. Same as Figure 8 but with convergence at the surface (white contours) and the column-averaged condensation rates (yellow contours) which are superimposed on the precipitation field. In panels (a) and (b), white contours are at 0.4 and 0.7 × 10^{-2} s^{-1} and

Deleted: 5
Deleted: A
Deleted:
Deleted: 6
Deleted: b
Deleted: c)
Deleted: d
Deleted: e
Deleted: in the control run and the low-aerosol run
Deleted: Panels (f) and (g) are the same as the panel (d) but the control-noevp run and the low-aerosol-noevp run are additionally displayed in Panel (f), while the control-homoge run and the low-aerosol-homoge run are additionally displayed in Panel (g).
Deleted: 7
Deleted: (blue contours), convergence at the surface (red contours), and the column-averaged condensation rates (black contours)
Deleted: rectangl
Deleted: es in Panels (c), (d), (e), (f), (g), and (h)
Deleted: In panels (a) and (b), red contours are at 0.4 and 0.7 × 10^{-2} s^{-1} and black contours are at 0.4 and 0.9 g m^{-3} h^{-1}. In panels (a) and (b), blue contours are at 10.0 and 30.0 mm h^{-1}. In panels (c) and (d), red contours are at 0.9 and 1.7 × 10^{-2} s^{-1}, black contours are at 0.9 and 1.5 g m^{-3} h^{-1}, and blue contours are at 10.0, 30.0, and 50.0 mm h^{-1}. In panels (e) and (f), red contours are at 1.4 and 2.3 × 10^{-2} s^{-1} and black contours are at 1.3 and 2.9 g m^{-3} h^{-1}. In panels (e) and (f), blue contours are at 10.0, 50.0, 100.0, and 130.0 mm h^{-1}. In panels (g) and (h), red contours are at 2.1 and 3.5 × 10^{-2} s^{-1} and black contours are at 2.3 and 3.8 g m^{-3} h^{-1}. In panels (g) and (h), blue contours are at 10.0, 30.0, 60.0, and 130.0 mm h^{-1}.
Deleted: 8
Deleted: 7
Deleted: runs
Deleted: Panel (c) shows the red line which marks the eastern part of where there is a substantial - reduction or transition from the high-value aerosol concentration of ~9000 cm^{-3} to the low-value aerosol concentration of ~700 cm^{-3}, as described in text related to Figure 4a, and the green rectangle at 19:00 LST.

yellow contours are at 0.4 and 0.9 g m^{-3} h^{-1}. In panels (c) and (d), white contours are at 0.9 and 1.7 × 10^{-2} s^{-1} and yellow contours are at 0.9 and 1.5 g m^{-3} h^{-1}. In panels (e) and (f), white contours are at 1.4 and 2.3 × 10^{-2} s^{-1} and yellow contours are at 1.3 and 2.9 g m^{-3} h^{-1}. In panels (g) and (h), white contours are at 2.1 and 3.5 × 10^{-2} s^{-1} and yellow contours are at 2.3 and 3.8 g m^{-3} h^{-1}.

Figure 11. Same as Figure 10 but with wind-vector fields (arrows) which are superimposed on the precipitation, convergence, and condensation fields.

Figure 12. Vertical distributions of the time- and domain-averaged (a) cloud-liquid and rain evaporation rates and (b) downdraft mass fluxes over each of the areas to the west and east of the strong convergence field for the control run and the low-aerosol run over a period between 17:00 and 19:00 LST (see text for details).

Figure 13. Spatial distributions of convergence (red contours) and wind vector (arrows) at the surface at 23:00 LST. Panels (a), (b), (c), and (d) are for the control-noevp run, the low-aerosol-noevp run, the control-homoge run, and the low-aerosol-homoge run, respectively, and contours are at 2.1 and 3.5 × 10^{-2} s^{-1}.

Deleted: Figure 9. Panels (a) and (b) are the same as Figures 7c and 7d, respectively, but with wind-vector fields (arrows) that are superimposed on the fields in Figures 7c and 7d. ¶
¶

Deleted: 0

Deleted: 1

Deleted: ¶
¶
¶
¶
¶
¶
¶
¶
¶

Simulations	Contrast in aerosol number concentration	The effect of cloud-liquid evaporation on temperature
Control run	Observed	Present
Low-aerosol run	Reduced by a factor of 2	Present
Control-noevp run	Observed	Absent
Low-aerosol-noevp run	Reduced by a factor of 2	Absent
Control-homoge run	Absent	Present
Low-aerosol-homoge run	Absent	Present

Table 1. Summary of simulations

Deleted: C

Formatted Table

Deleted: ¶
spatial distribution

Deleted: Observed

Deleted: Reduced by a factor of 2

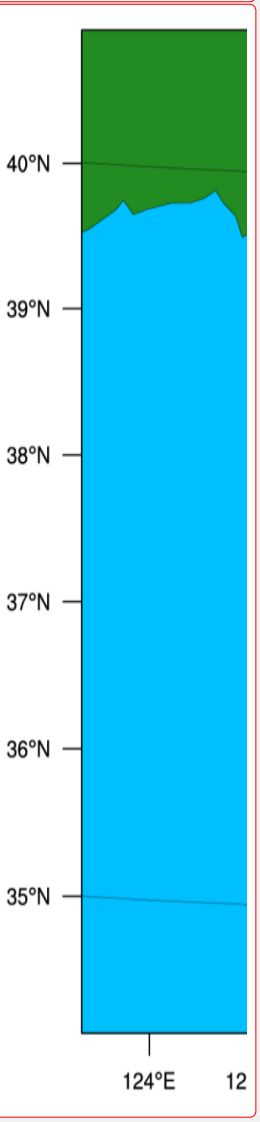

Deleted:

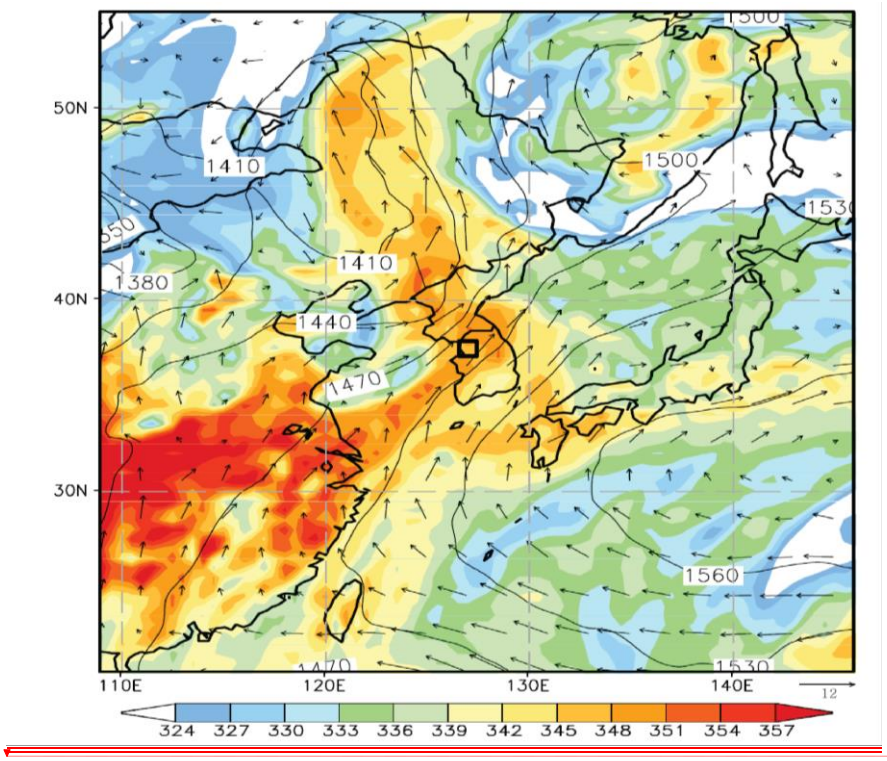

Moved (insertion) [2]

Figure 1

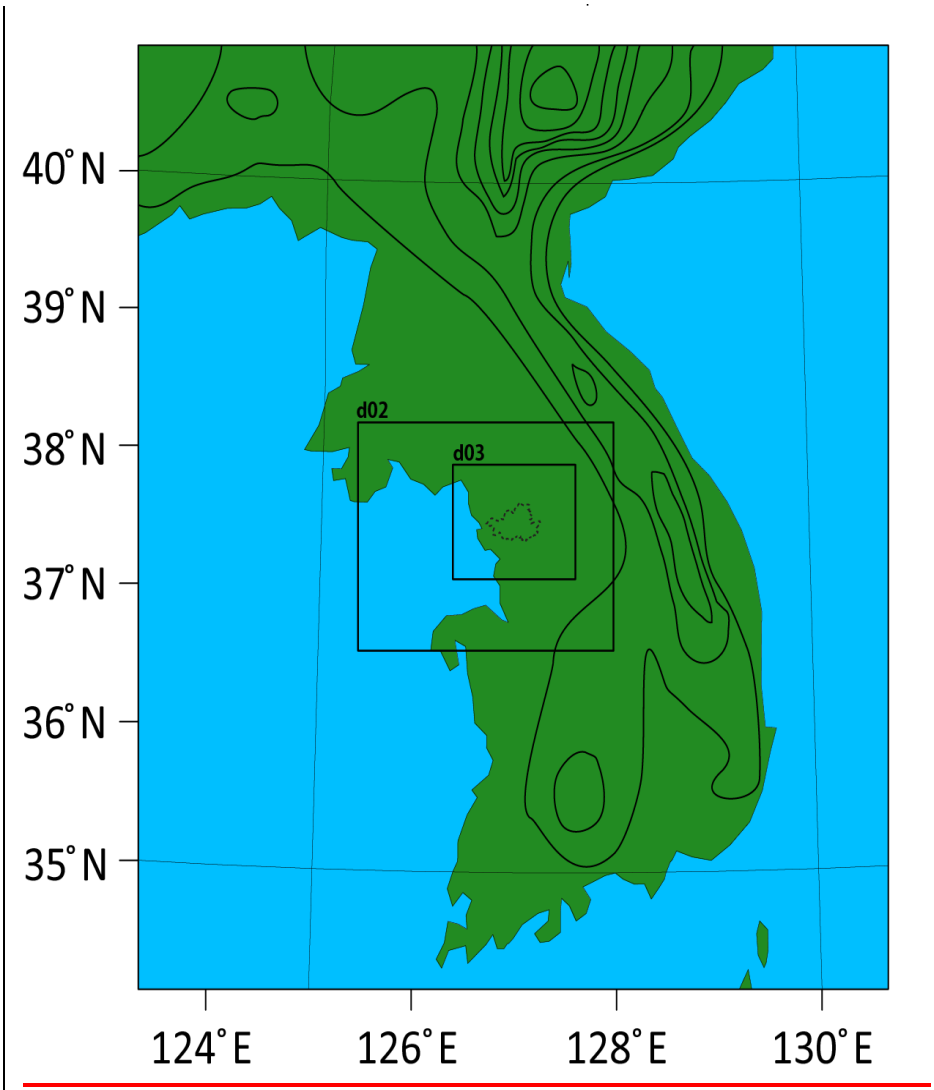

Figure 2

Deleted: 1

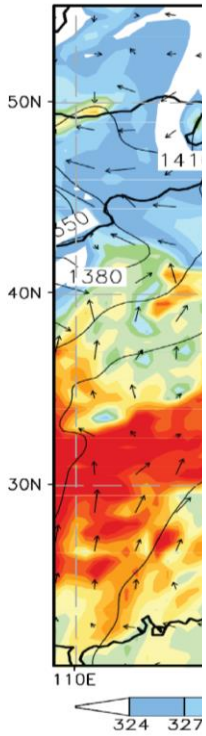

Moved up [2]:

Deleted: Figure 2¶

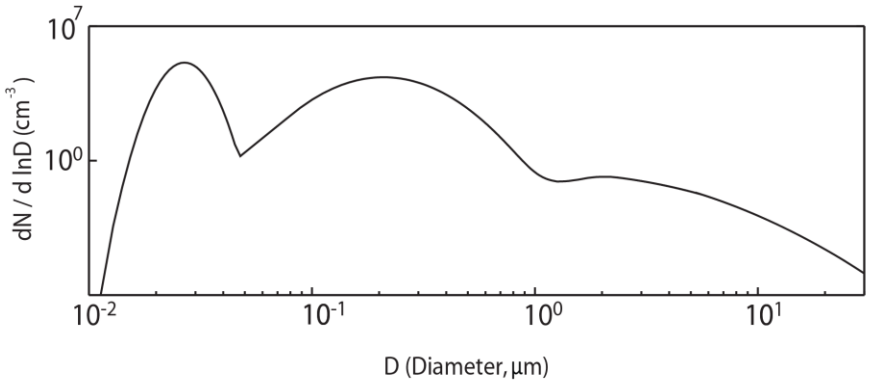

Figure 3

Deleted: 3

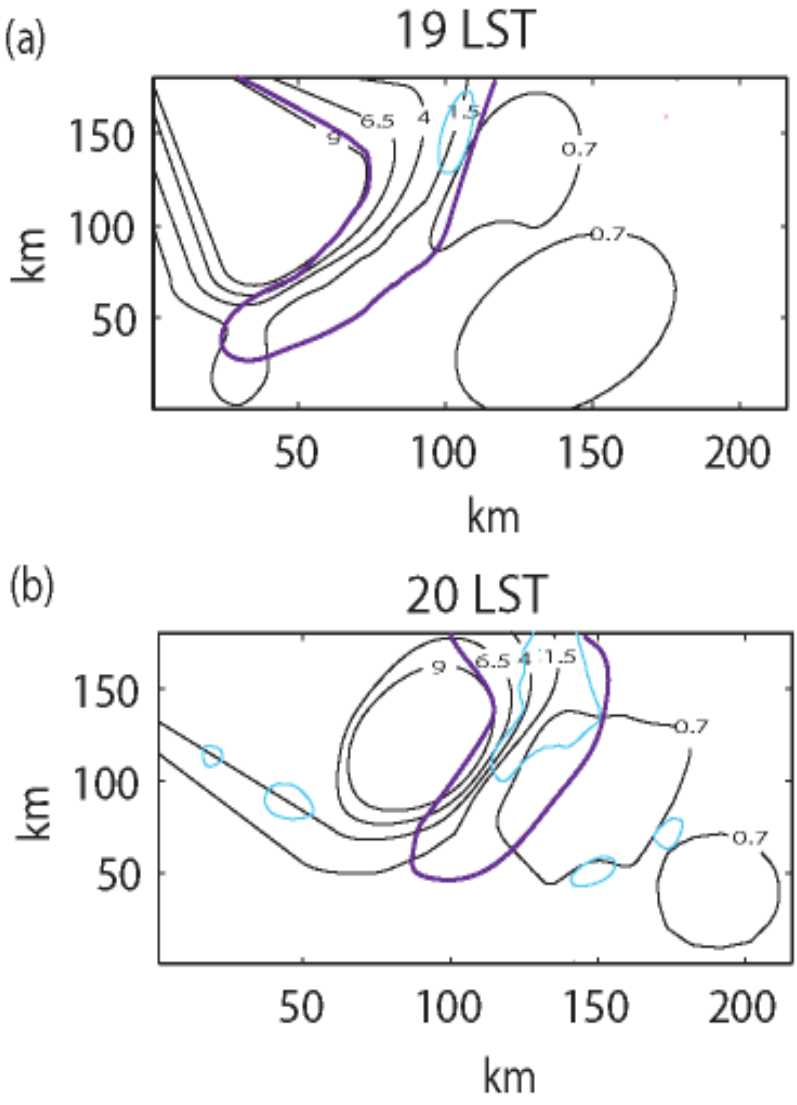

2093

2094 **Figure 4**

2095

Deleted:

Deleted: 4

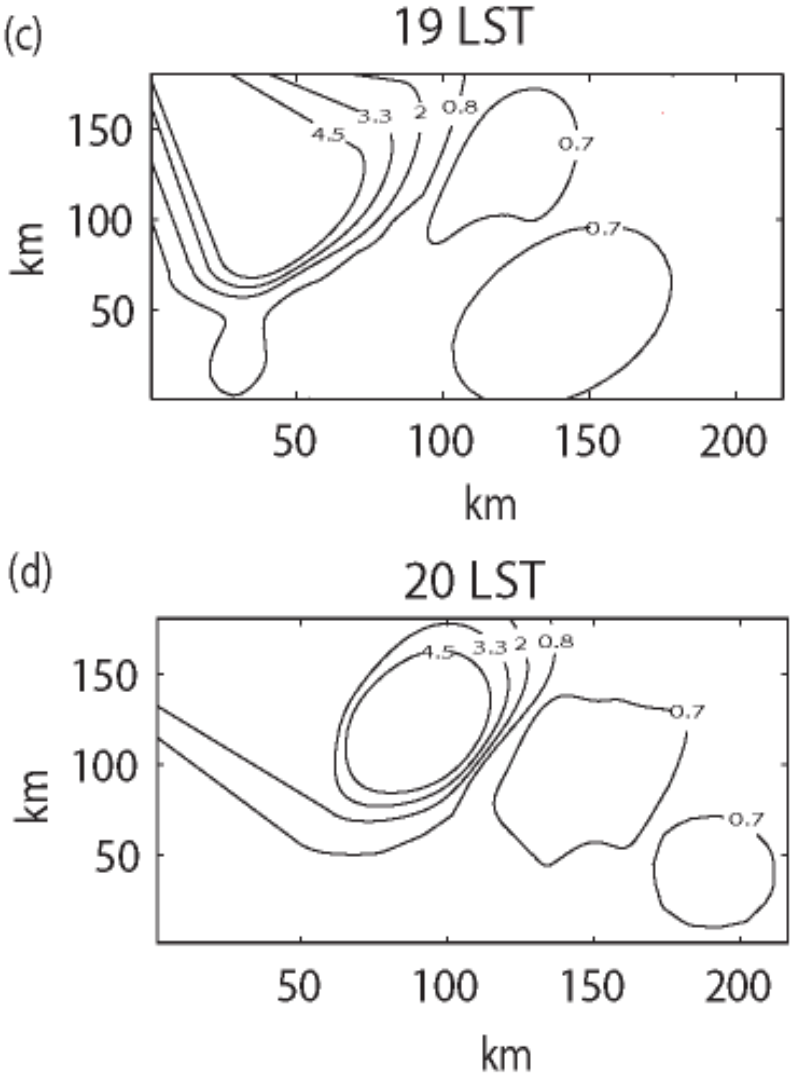

Figure 4

Deleted: 4

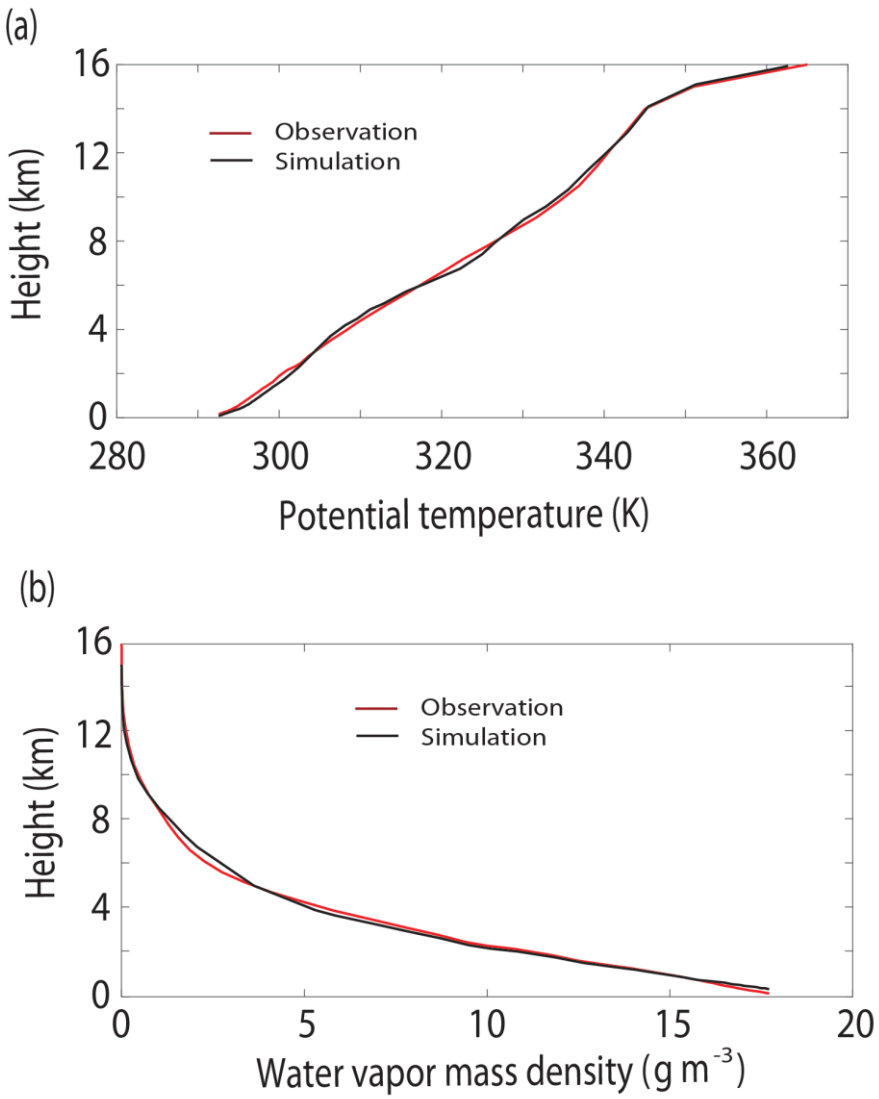
(a)
Height (km)
16
12
8
4
0
280
300
320
340
360
Potential temperature (K)
Observation
Simulation
(b)
Height (km)
16
12
8
4
0
0
5
10
15
20
Water vapor mass density (g m^{-3})
Observation
Simulation

Figure 5

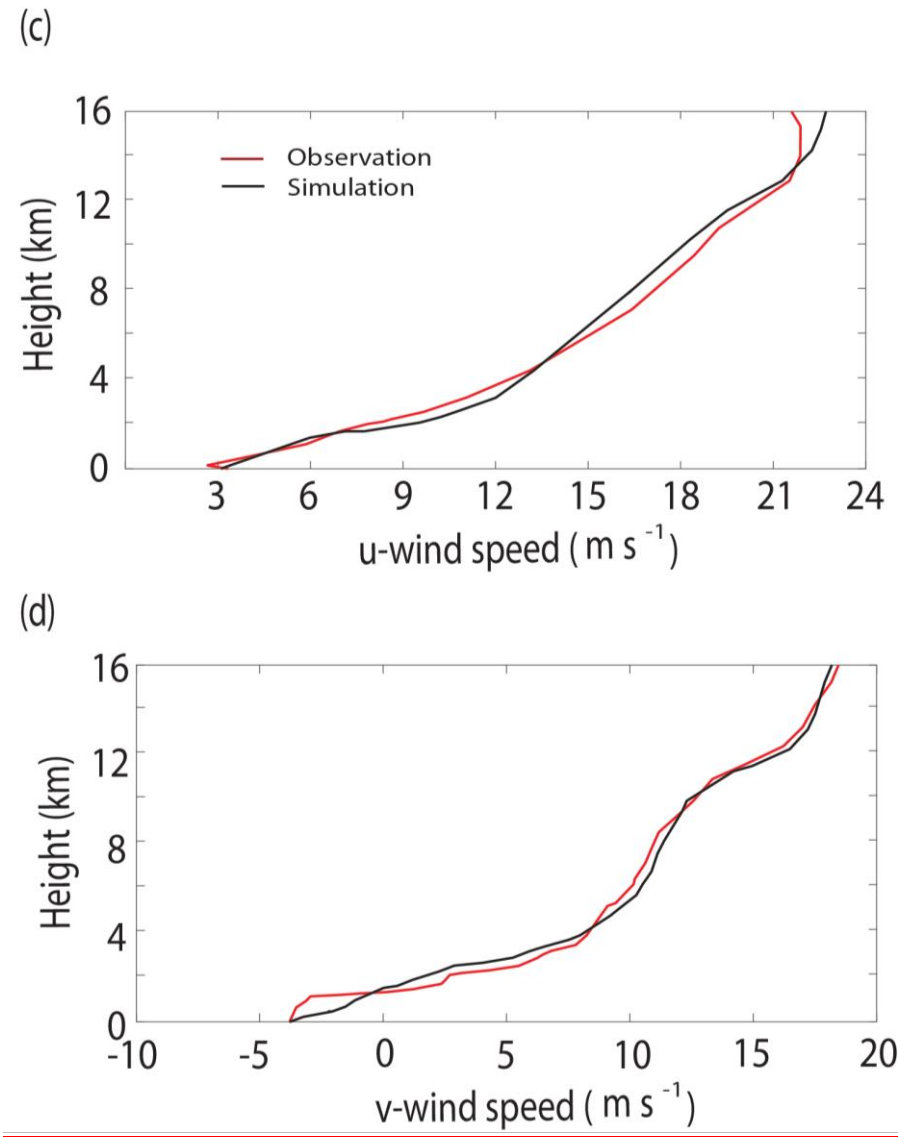
(c)
Observation
Simulation
Height (km)
u-wind speed (m s -1)
(d)
Height (km)
v-wind speed (m s -1)

Figure 5

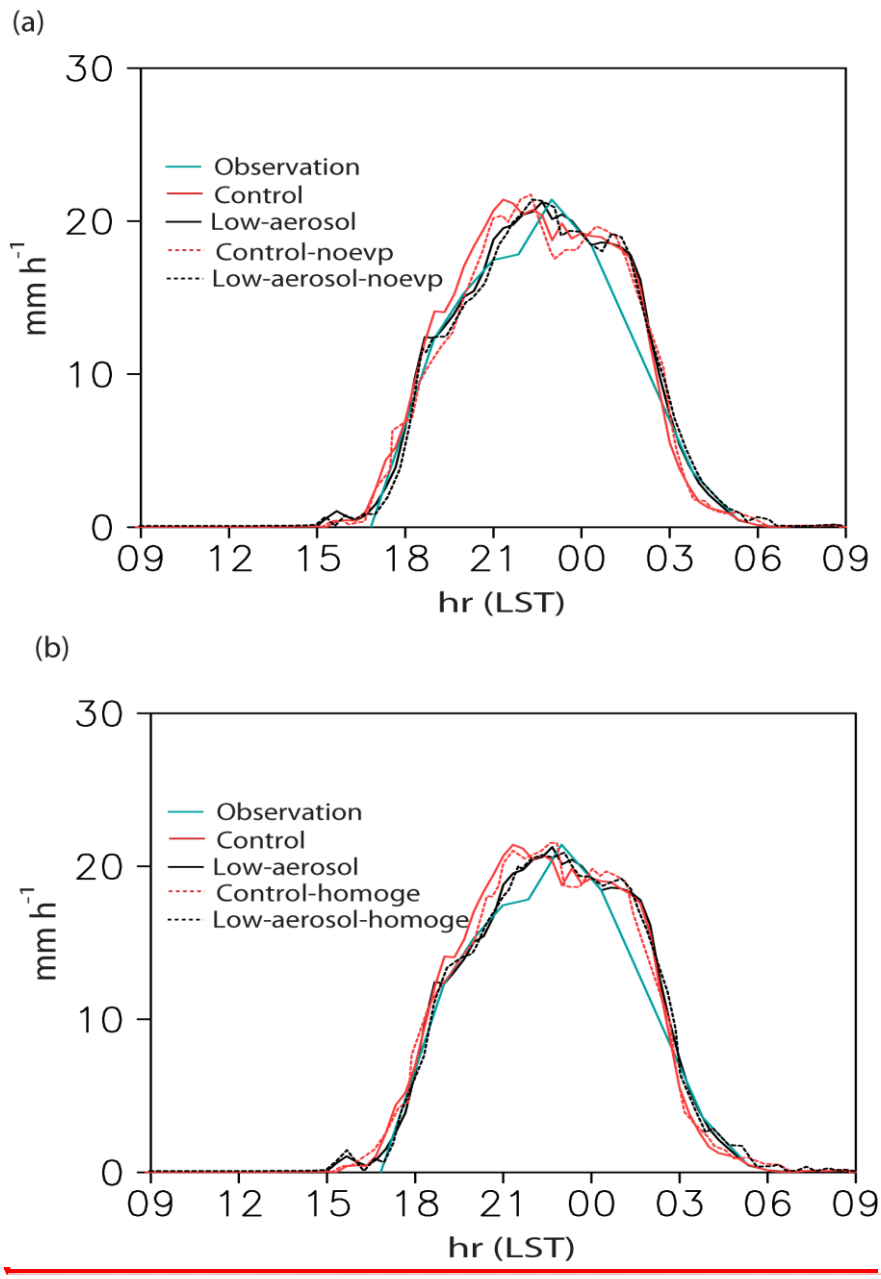

Deleted:

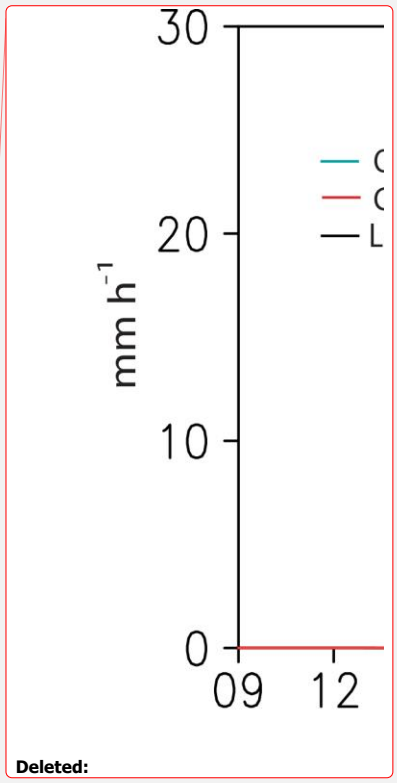

Deleted:

2110

2111 **Figure 6**

Deleted:

Deleted: 5

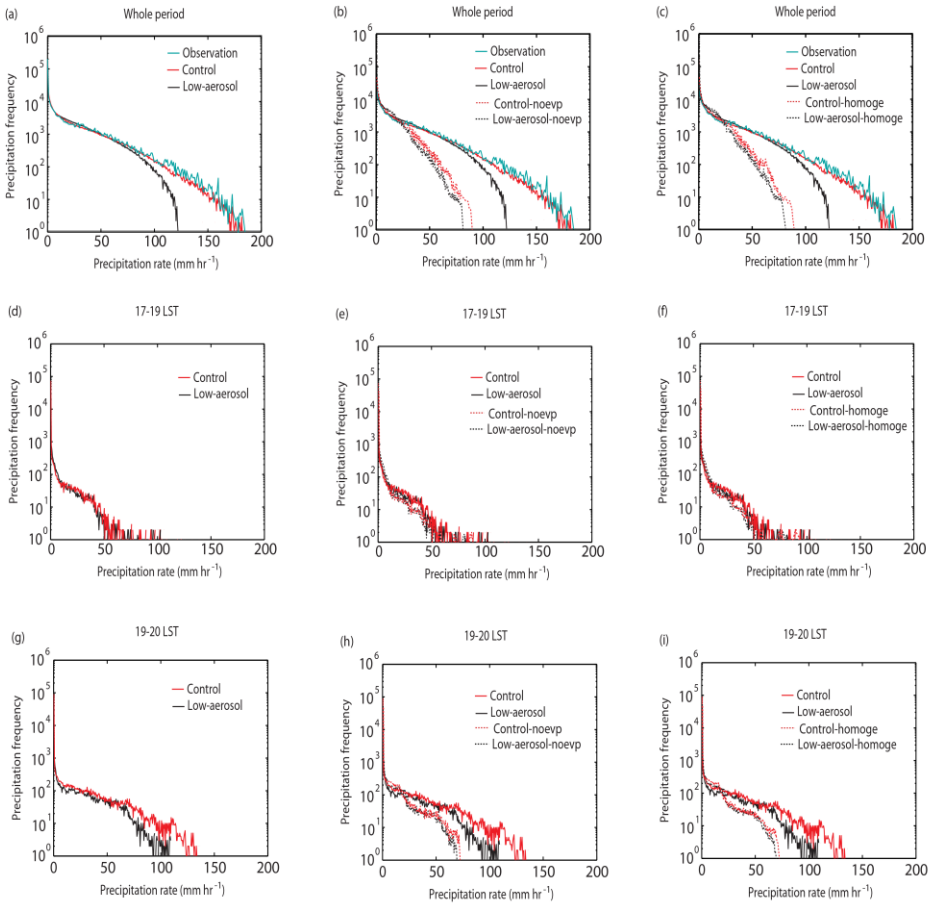
(a)
Whole period
Observation
Control
Low-aerosol
(b)
Whole period
Observation
Control
Low-aerosol
Control-noevp
Low-aerosol-noevp
(c)
Whole period
Observation
Control
Low-aerosol
Control-homoge
Low-aerosol-homoge
(d)
17-19 LST
Control
Low-aerosol
(e)
17-19 LST
Control
Low-aerosol
Control-noevp
Low-aerosol-noevp
(f)
17-19 LST
Control
Low-aerosol
Control-homoge
Low-aerosol-homoge
(g)
19-20 LST
Control
Low-aerosol
(h)
19-20 LST
Control
Low-aerosol
Control-noevp
Low-aerosol-noevp
(i)
19-20 LST
Control
Low-aerosol
Control-homoge
Low-aerosol-homoge
Precipitation frequency
Precipitation rate (mm hr-1)

Figure 7

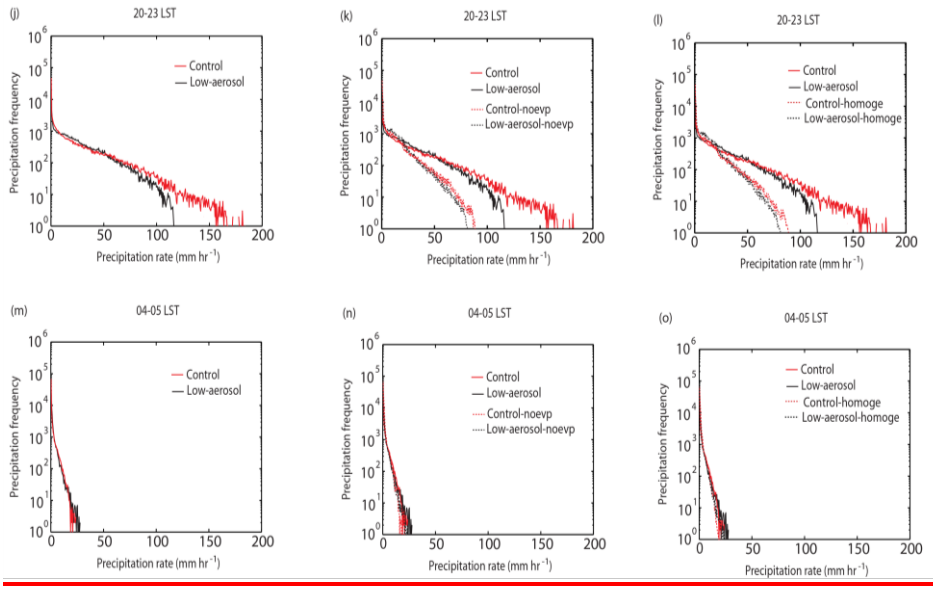

Figure 7

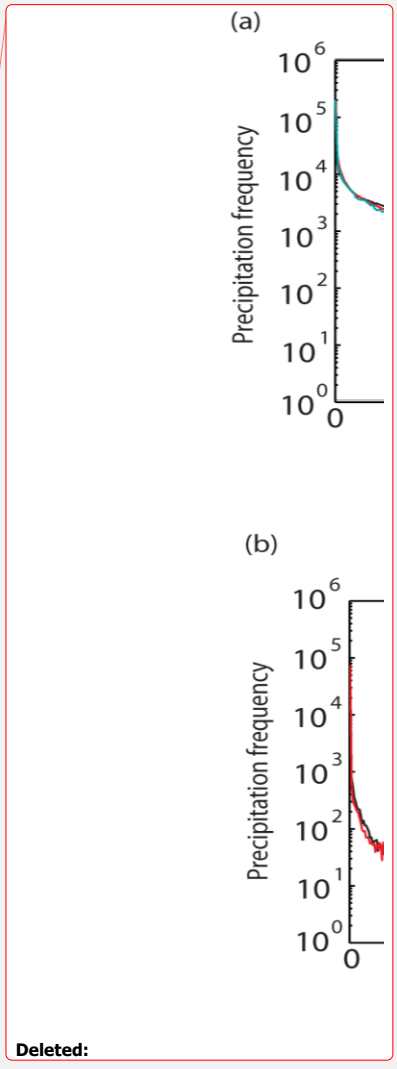

Deleted:

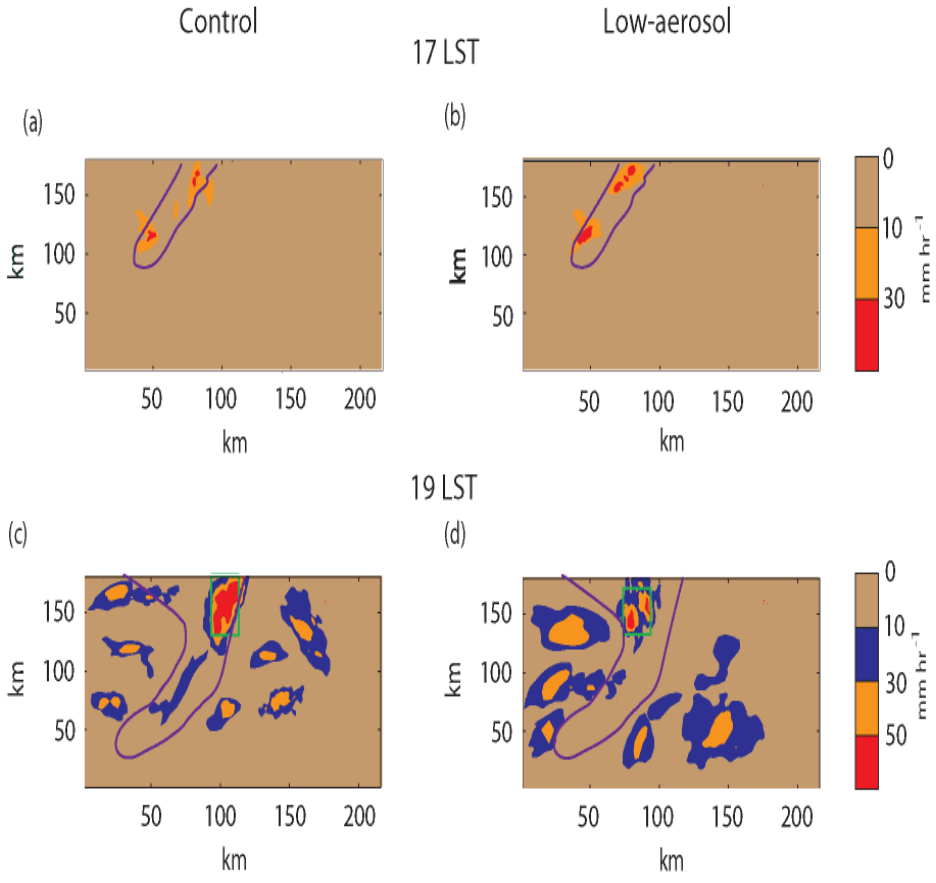

Figure 8

Deleted:

Deleted: 6

Deleted: ¶

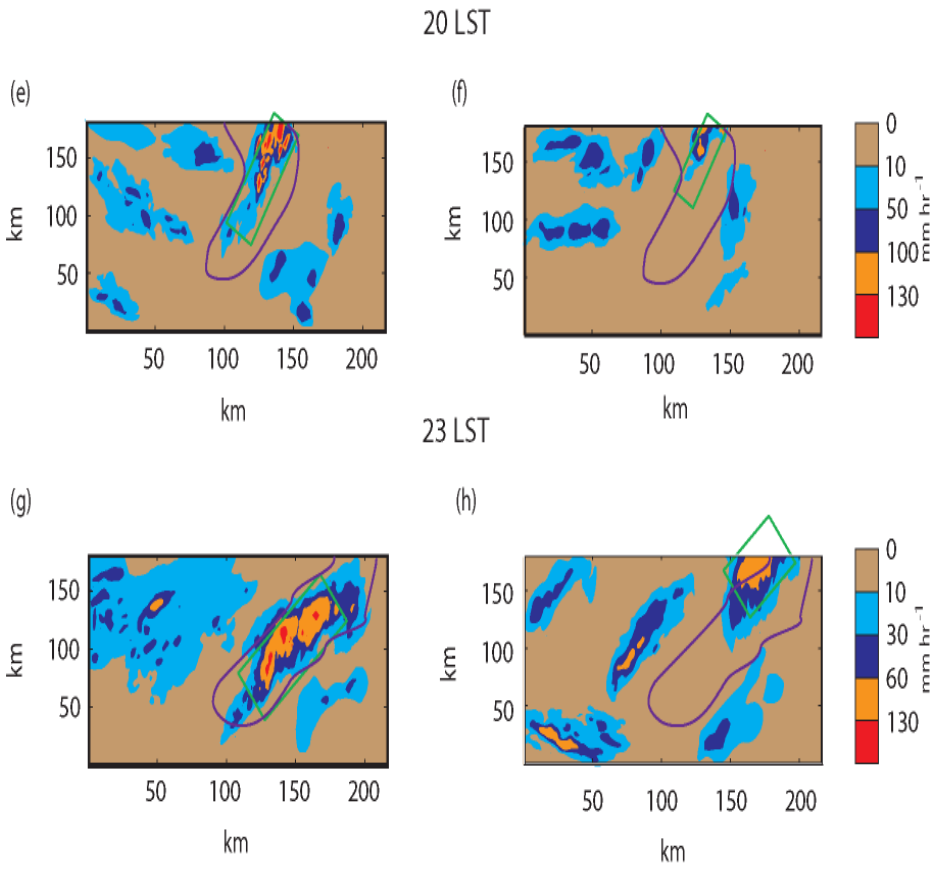

Figure 8

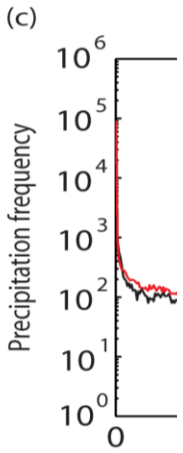

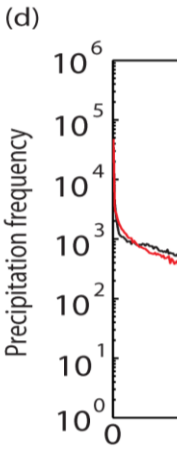

Deleted: Figure 6¶

¶

¶

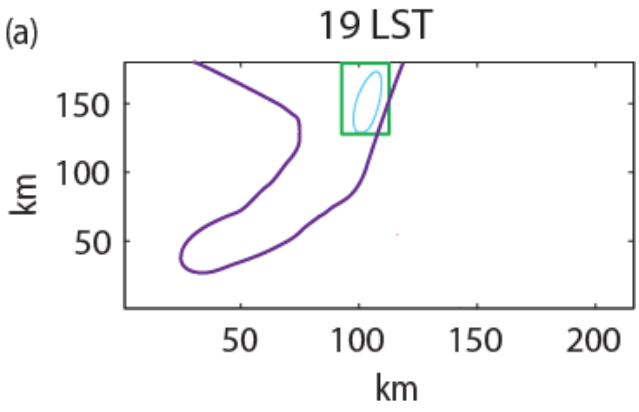

Figure 9

Deleted:

Deleted: 8

Control

Deleted:

Moved down [3]:
Figure 9¶

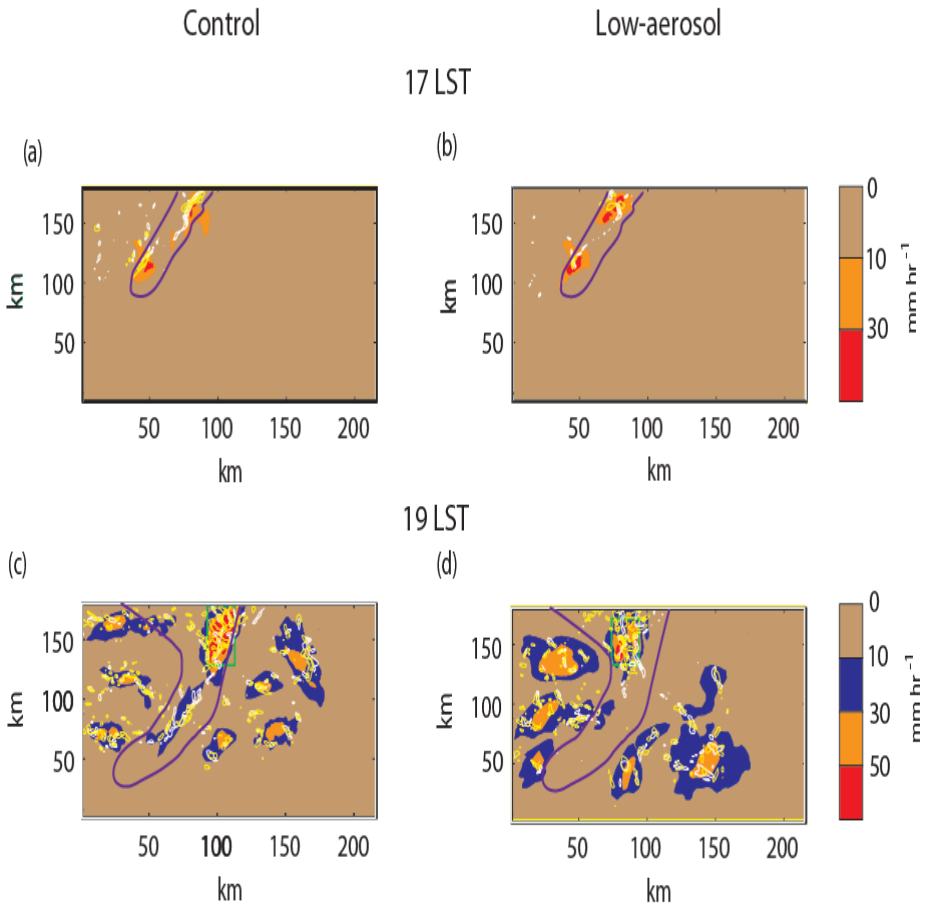

Figure 10

Moved (insertion) [3]

Deleted:

Deleted: 9

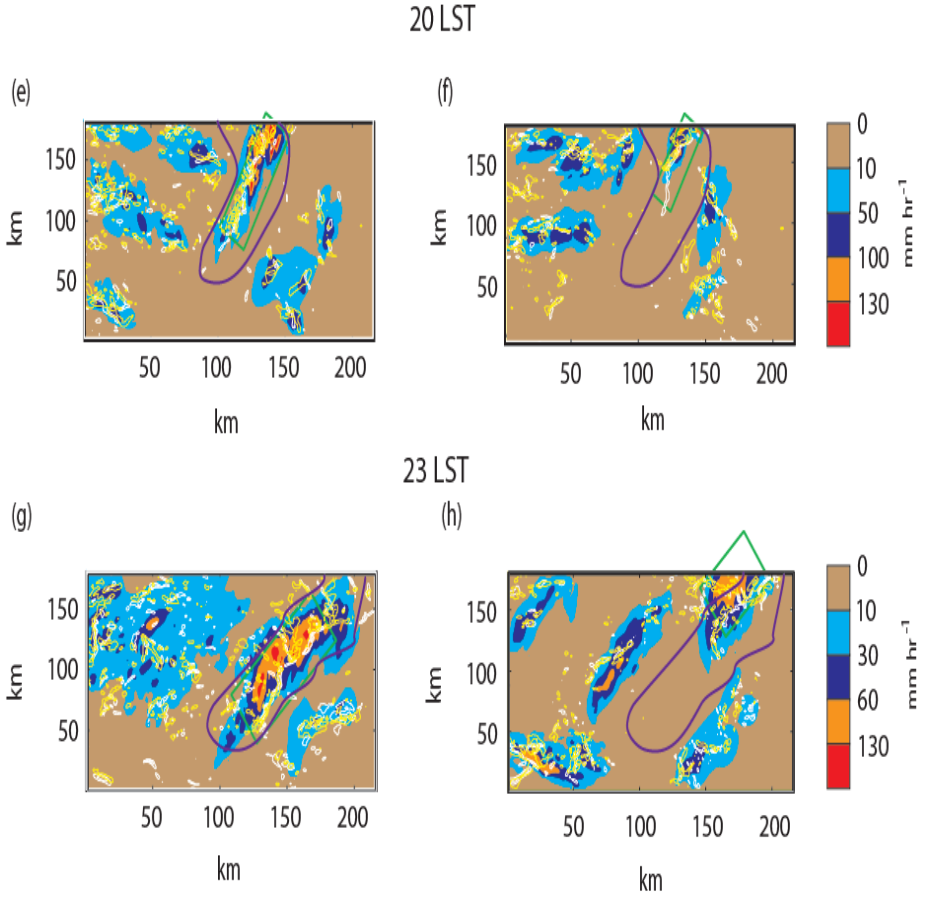
20 LST
(e)
(f)
150
100
50
km
50
100
150
200
km
0
10
50
100
130
mm hr⁻¹
23 LST
(g)
(h)
0
10
30
60
130

Figure 10

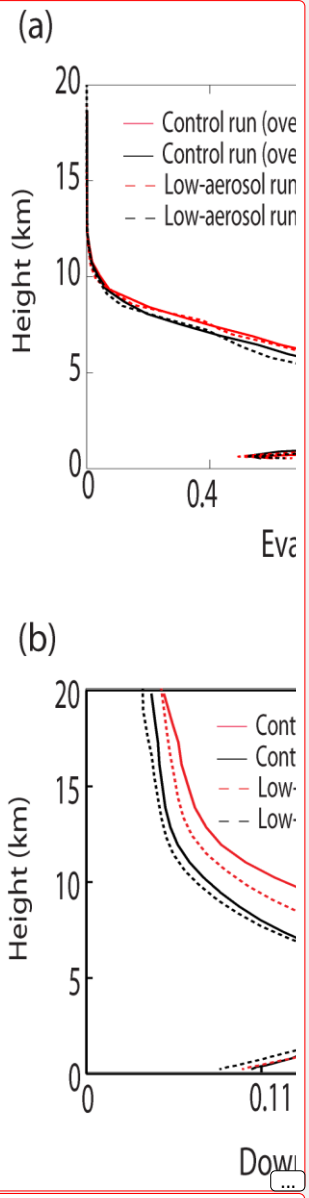
(a)
Height (km)
Control run (ove
Control run (ove
Low-aerosol run
Low-aerosol run
0.4
(b)
Cont
Cont
Low·
Low·
0.11

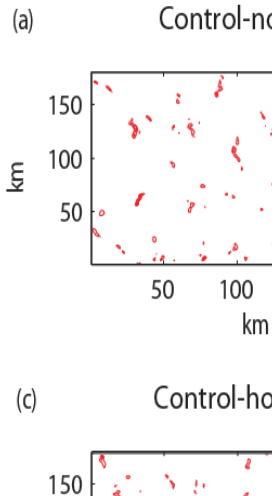
(a)
Control-nc
km
(c)
Control-ho

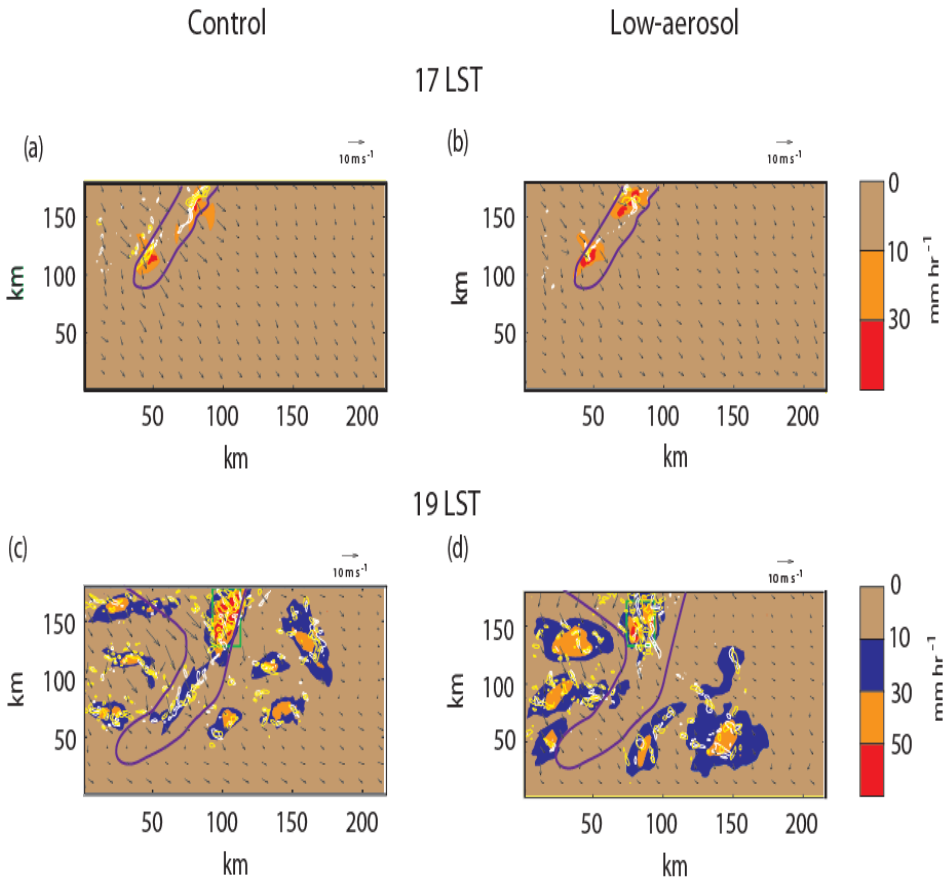
Control
Low-aerosol
17 LST
(a)
(b)
19 LST
(c)
(d)
10 m s-1
km
150
100
50
200
0
10
30
50
mm hr-1

Figure 11

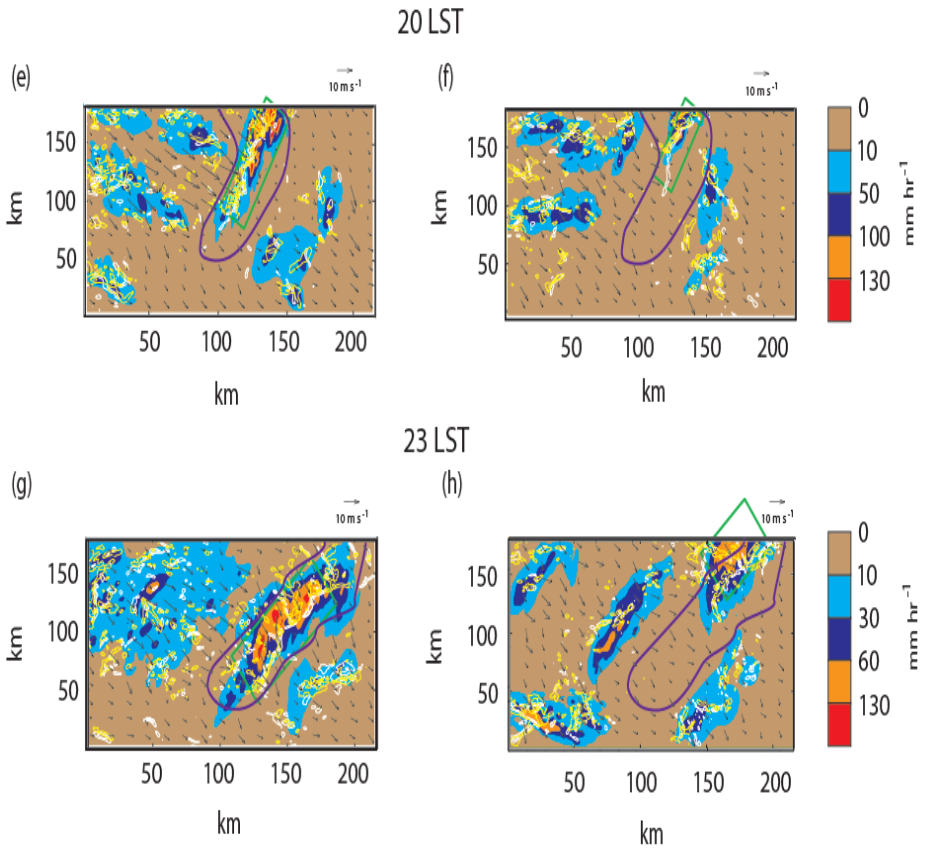
20 LST
(e)
(f)
10 ms-1
km
150
100
50
50
100
150
200
0
10
50
100
130
mm hr-1
23 LST
(g)
(h)
0
10
30
60
130

Figure 11

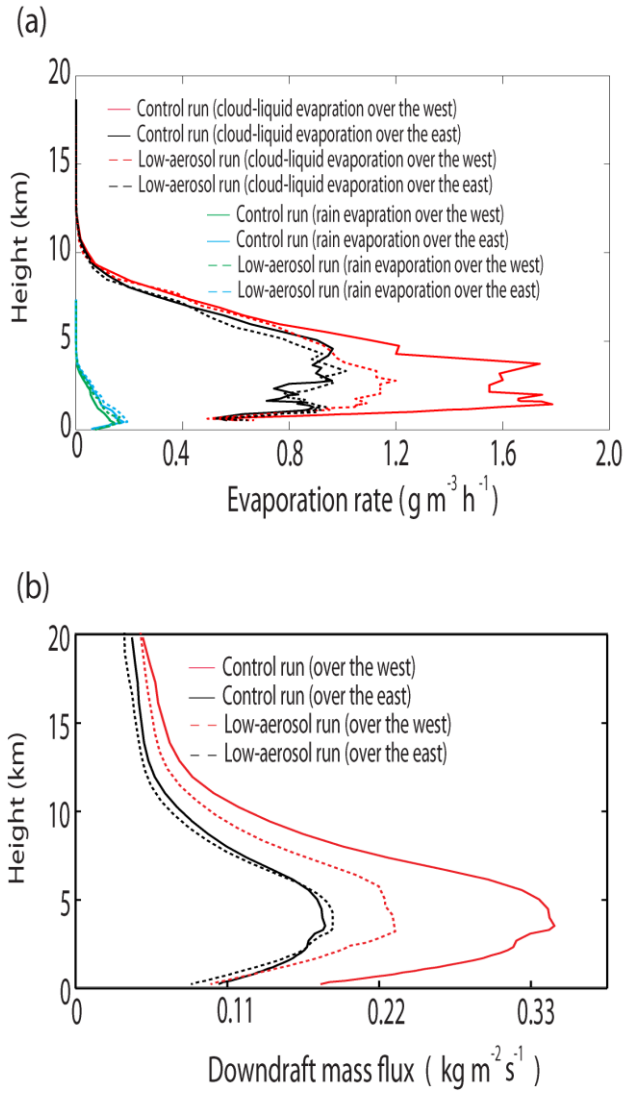
(a)
Height (km)
Evaporation rate (g m-3 h-1)
Control run (cloud-liquid evapration over the west)
Control run (cloud-liquid evaporation over the east)
Low-aerosol run (cloud-liquid evaporation over the west)
Low-aerosol run (cloud-liquid evaporation over the east)
Control run (rain evapration over the west)
Control run (rain evaporation over the east)
Low-aerosol run (rain evaporation over the west)
Low-aerosol run (rain evaporation over the east)
(b)
Height (km)
Downdraft mass flux (kg m-2 s-1)
Control run (over the west)
Control run (over the east)
Low-aerosol run (over the west)
Low-aerosol run (over the east)

Figure 12

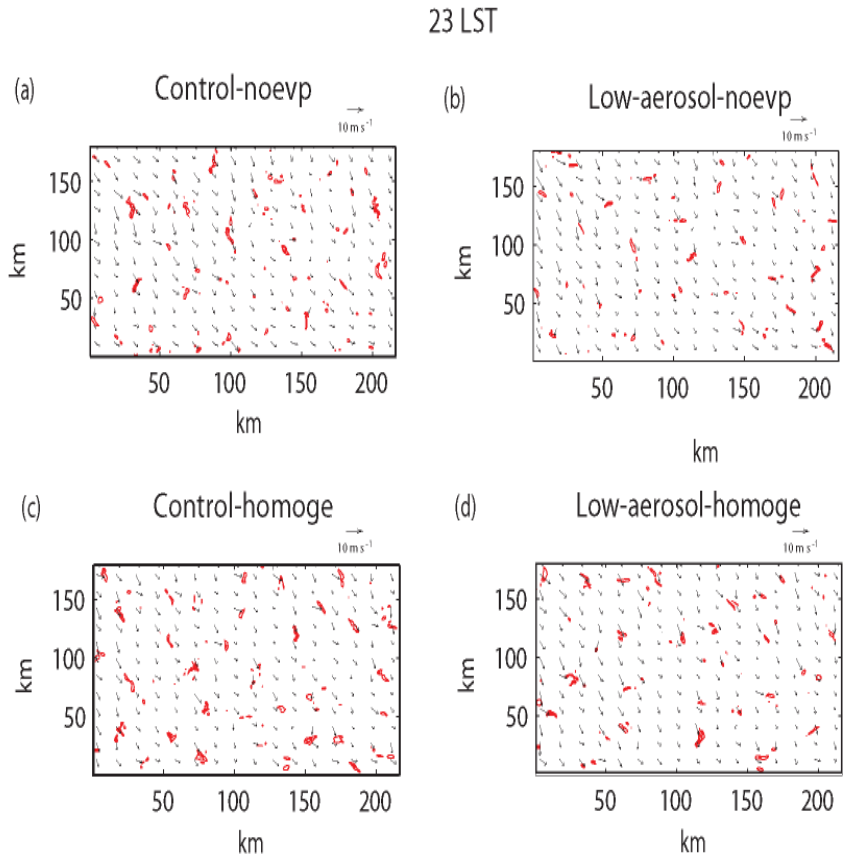

Figure 13

Deleted:

Deleted: 11

Deleted: ¶